Molecular Neurobiology
https://doi.org/10.1007/s12035-024-04495-9

RESEARCH

Inhibition of Phosphodiesterase 4 Suppresses Neuronal Ferroptosis After Cerebral Ischemia/Reperfusion

Kechun Chen[1] · Bingtian Xu[1] · Lu Long[1] · Huizhen Wen[1] · Qian Zhao[1] · Xingxing Tu[1] · Jiakang Wang[1] · Jiangping Xu[1,2,3] · Haitao Wang[1]

Received: 10 March 2024 / Accepted: 12 September 2024

Abstract

We have previously shown that inhibition of phosphodiesterase 4 (PDE4) protects against cerebral ischemia/reperfusion injury. However, it remains unclear whether and how PDE4 affects ferroptosis under cerebral ischemia/reperfusion conditions. In this study, we found that overexpression of PDE4B in HT-22 cells exacerbated the detrimental effects of oxygen–glucose deprivation/reoxygenation (OGD/R), including a decrease in cell viability and glutathione (GSH) levels and an increase in Fe^{2+} content. PDE4B knockdown mitigated the effects of OGD/R, as evidenced by decreased oxidative stress, lactate dehydrogenase (LDH) release, Fe^{2+} content, and nuclear receptor coactivator 4 (NCOA4) expression. PDE4B knockdown also enhanced the levels of GSH, ferroportin (FPN), and ferritin heavy chain 1 (FTH1). Consistently, inhibition of PDE4 by roflumilast (Roflu) produced similar effects as PDE4B knockdown. Roflu also ameliorated the morphology and membrane potential of the mitochondria. Glutathione peroxidase 4 (GPX4) knockdown blocked the effects of Roflu on cell viability and lipid peroxidation. Moreover, we found that nuclear factor erythroid 2-related factor 2 (Nrf-2) knockdown decreased GPX4 expression. In addition, Nrf-2 knockdown led to enhanced lipid peroxidation, LDH release, and iron levels, while the GSH and FPN levels decreased. More crucially, PDE4 inhibition decreased infarct volume, alleviated oxidative stress, and restored the expression levels of ferroptosis-associated proteins in middle cerebral artery occlusion/reperfusion (MCAO/R) rats. Interestingly, the GPX4 inhibitor RSL3 blocked the neuroprotective effects of Roflu in rats subjected to MCAO/R. Thus, PDE4 inhibition significantly inhibits neuronal ferroptosis by activating the Nrf-2/GPX4 pathway. These data indicate the existence of a novel mechanism underlying the neuroprotective effects of PDE4 inhibition.

Keywords PDE4 · Ferroptosis · Oxidative Stress · Iron · Cerebral Ischemia · Nrf-2

Introduction

Ischemic stroke is one of the leading causes of death as well as disability worldwide [1]. Although some progress has been made in the research on ischemic brain injury in recent years, the number of therapeutic agents for ischemic stroke is still very limited [2]. Recombinant tissue plasminogen activator is an FDA-approved drug for the treatment of ischemic stroke [3]. However, its narrow therapeutic window and the disadvantage of possible bleeding greatly limit its clinical application [3]. Hence, there is an urgent need to further clarify the mechanism of neuronal death in ischemic brain injury and to identify novel therapeutic targets and drugs for the treatment of ischemic stroke.

Phosphodiesterase 4 (PDE4) is a specific hydrolase responsible for the hydrolysis of the second messenger cyclic adenosine monophosphate (cAMP). Inhibition

Kechun Chen and Bingtian Xu contributed equally to this work.

✉ Haitao Wang
wht821@smu.edu.cn

1 NMPA Key Laboratory for Research and Evaluation of Drug Metabolism & Guangdong Provincial Key Laboratory of New Drug Screening, School of Pharmaceutical Sciences, Southern Medical University, Guangzhou 510515, China

2 Key Laboratory of Mental Health of the Ministry of Education, Southern Medical University, Guangzhou 510515, China

3 Center for Brain Science and Brain-Inspired Intelligence, Guangdong-Hong Kong-Macao Greater Bay Area, Guangzhou 510515, China

Published online: 17 September 2024

of PDE4 increases the intracellular level of cAMP and activates multiple signaling pathways [4]. Studies by our group and other researchers have previously demonstrated that targeting PDE4 by either gene knockout or small molecule inhibitors increases neuronal survival in a variety of neurological disease models [5, 6]. Our previous study showed that PDE4 inhibition ameliorates cognitive deficits in APP/PS1 transgenic mice [7]. We also found that PDE4 inhibitors protected dopaminergic neurons against apoptosis in experimental models of Parkinson's disease [8]. Recently, we demonstrated the involvement of PDE4 in neuronal death in ischemic brain injury [9]. Interestingly, we found that inhibition of PDE4 reduced the levels of reactive oxygen species (ROS) in neurons under ischemic and hypoxic conditions [10]. The above studies have shown that PDE4 is a potential target for the treatment of central nervous system diseases. In addition, revealing the mechanism by which inhibition of PDE4 produces neuroprotective effects will facilitate the discovery of novel targets and drugs for the treatment of cerebral ischemia.

Iron-dependent excessive lipid peroxidation and mitochondrial dysfunction are characteristics of ferroptosis, which is a novel form of regulated cell death first described in 2012 [11]. Ferroptosis is closely associated with the initiation and progression of ischemic stroke [12]. In an animal model of middle cerebral artery occlusion/reperfusion (MCAO/R), iron overload was observed in the ischemic penumbra, and attenuation of ferroptosis alleviated iron overload and cerebral infarction caused by MCAO/R [13]. Consistently, iron levels in serum are significantly elevated in patients with ischemic stroke [14]. Intracellular polyunsaturated fatty acids undergo a Fenton reaction in the presence of divalent iron ions, generating large amounts of ROS, which in turn induce cell death, and intracellular mitochondrial sequestration is observed morphologically [15]. Therefore, from this perspective, ferroptosis may be inhibited by modulating intracellular iron homeostasis, reducing ROS levels and lipid peroxidation. Emerging studies have reported that ferroptosis deteriorates cerebral ischemia and that inhibition of ferroptosis is beneficial for the treatment of stroke [16–18]. In summary, targeting ferroptosis is a potential strategy for the treatment of ischemic brain injury. Our previous study indicated that inhibition of PDE4 attenuates the production of ROS in neurons. Importantly, inhibition of PDE4 enhances the translocation of nuclear factor erythroid 2-related factor 2 (Nrf-2) from the cytoplasm into the nucleus and activates Nrf-2 in neurons under oxygen–glucose deprivation/reoxygenation (OGD/R) conditions [19]. Nrf-2 has been proven to play a pivotal role in the regulation of ferroptosis [20]. However, whether PDE4 is involved in the regulation of ferroptosis during the process of stroke is unknown.

The aim of the present study was to evaluate the protective role of PDE4 inhibition against ferroptosis induced by cerebral ischemia and to identify the underlying signaling pathways. Based on our previous studies, we hypothesized that specific inhibition of PDE4 would protect against neuronal ferroptosis. Mechanistically, the anti-ferroptotic effects of PDE4 inhibition would be mediated through the activation of Nrf-2. In the present study, we exposed HT-22 neuronal cells to OGD/R and examined the changes in the expression of ferroptosis markers, iron-related parameters, and potential signaling pathways. We also verified the role of PDE4 inhibition in rats subjected to MCAO/R. Collectively, our study identified PDE4 as a novel contributor involved in ferroptosis during the process of stroke. Additionally, roflumilast (Roflu), an FDA-approved drug for the treatment of chronic obstructive pulmonary disease, is a pan-PDE4 inhibitor with a subnanomolar IC_{50} value against PDE4 activity [21]. In the present study, we also found that Roflu is a potent neuroprotective agent against ferroptosis-associated diseases including cerebral ischemia.

Materials and Methods

Materials

Roflu (#S2131) and z-VAD-fmk (Zvad, #S7023) were obtained from Selleck (Shanghai, China). An Image-iT™ Lipid Peroxidation Kit (#C10445), Lipofectamine™ 3000 Transfection Reagent (#L3000008), Opti-MEM® Reduced-Serum Medium (#31985088), CellROX Deep Red Reagent (#C10422), a Click-iT™ Lipid Peroxidation Imaging Kit (#C10446), and tetramethylrhodamine ethyl ester perchlorate (TMRE, #T669) were obtained from Thermo Fisher Scientific (Waltham, MA, USA). Antibodies against cyclooxygenase-2 (COX2, #12282), ferritin heavy chain 1 (FTH1, #4393), and PDE4B (#72096) were purchased from Cell Signaling Technology, Inc. (Massachusetts, USA). Antibodies against glutathione peroxidase 4 (GPX4, #ab125066), acyl-CoA synthetase long-chain family member 4 (ACSL4, #ab155282), and nuclear receptor coactivator 4 (NCOA4, #ab86707) were obtained from Abcam (Cambridge, UK). Antibodies against ferroportin (FPN, #26601–1-AP) and Nrf-2 (#16396–1-AP) were obtained from Proteintech (Wuhan, Hubei, China). An antibody against glyceraldehyde-3-phosphate dehydrogenase (GAPDH, #FD0063) was obtained from Fude Biological Technology (Hangzhou, China). Small interfering RNAs (si-RNAs) specific to GPX4, Nrf-2, and PDE4B were obtained from GenePharma (Shanghai, China). The PDE4B plasmid was constructed by Shuangquan Biotechnology (Guangzhou, Guangdong, China), and the lipid peroxidation malondialdehyde (MDA) assay kit (#S0131) and lactate dehydrogenase (LDH) assay

kit (#C0017) were purchased from Beyotime Biotechnology (Shanghai, China). 2,3,5-Triphenyltetrazolium chloride (TTC, #T8877) was purchased from Merck (Darmstadt, Germany). A Cell Counting Kit-8 (CCK-8, #CK04) and FerroOrange (#F374) were obtained from Dojindo Molecular Technologies (Tokyo, Japan). Ferrostatin-1 (Fer-1, #F129882) and erastin (#E126853) were purchased from Aladdin (Shanghai, China). Deferoxamine mesylate (DFO, #D873692), RSL3 (#R873890), and the autophagy inhibitor chloroquine (CQ, #C843545) were purchased from Macklin (Shanghai, China). An iron assay kit (#E-BC-K139-S) was obtained from Elabscience Biotechnology (Wuhan, China), and a glutathione (GSH) assay kit (#A006-2–1) was obtained from the Nanjing Jiancheng Bioengineering instituteInstitute (Nanjing, China). Polyoxyl 15 hydroxystearate (HS-15, #MB1809-1) was purchased from Meilunbio (Dalian, China).

Cell Culture

The HT-22 cell line was purchased from Merck (Darmstadt, Germany). The cells were cultured in DMEM (#11965092, Thermo Fisher Scientific) containing 10% fetal bovine serum (FBS, #A3161001C, Thermo Fisher Scientific) in an incubator with 5% CO_2 and 95% air at 37 °C.

Animals

Male adult (260–290 g) Sprague–Dawley rats were purchased from the Experimental Animal Center of Southern Medical University (Guangzhou, Guangdong, China). The temperature was maintained at 20–24 °C. The relative humidity was maintained at 55–65%. All experimental procedures were approved by the Laboratory Animal Ethics Committee of Southern Medical University (approval number: SMUL202310009) and performed in compliance with the ethical guidelines of the NIH Guide for the Care and Use of Laboratory Animals (NIH, revised 1996).

Drug Preparation

For in vivo experiments, the PDE4 inhibitor Roflu was dissolved in 0.9% saline containing 5% Tween-80 and 0.5% dimethyl sulfoxide (DMSO). The apoptosis inhibitor Zvad, the necrosis inhibitor Nec-1, the autophagy inhibitor CQ, the ferroptosis inducers RSL3 and erastin, and the ferroptosis inhibitor Fer-1 were dissolved in DMSO and diluted in a cell culture medium. The ferroptosis inhibitor DFO was dissolved in PBS and diluted in a cell culture medium. For in vitro experiments, Roflu and RSL3 were dissolved in 0.9% saline containing 5% absolute ethyl alcohol and 5% HS-15.

Oxygen–glucose Deprivation Cell Model

The oxygen–glucose deprivation cell model was established using HT-22 cells as previously described [22]. HT-22 cells were seeded in plates or dishes. After cells were adhered, they were washed with PBS twice, and then the medium was changed to serum- and glucose-free DMEM (#11966025, Thermo Fisher Scientific). The cells were transferred to an anoxic chamber with 95% N_2 and 5% CO_2 at 37ºC. The control cells were cultured in normal DMEM in a normal cell incubator. After 6 h, the cells were transferred from the anoxic chamber to the normal cell incubator, and the medium was changed to DMEM.

Cell Viability Assay

Cell viability was determined by the CCK-8 assay. HT-22 cells were seeded at a density of 70–80%. The next day, the cells were exposed to OGD/R, and then 20 μL of CCK-8 reagent was added to each well, and cells were incubated at 37ºC. Finally, the absorbance at 450 nm was determined by a microplate reader (BioTek Synergy HTX).

LDH Release Assay

HT-22 cells were seeded at a density of 70–80%. The next day, the cells were exposed to OGD/R. Next, 120 μl of the medium was collected and transferred to a 96-well plate. Then 60 μl of LDH detection working liquid (lactic acid solution:INT solution:enzyme solution, 1 : 1 : 1) was added to each well. The 96-well plate was placed on a shaker at room temperature away from light for 30 min. Finally, the absorbance at 490 nm was determined by a microplate reader.

PDE4B Plasmid Transfection

Plasmid transfection was performed as previously described [19]. Briefly, the PDE4B plasmid and P3000™ reagent were mixed in opti-MEM, while Lipofectamine™ 3000 was mixed with opti-MEM in another tube. After incubation at room temperature for 5 min, these two were mixed gently, incubated at room temperature for 20 min, and added to the cells. Subsequent experiments were carried out after incubation for 24 h.

Transfection of siRNA

The si-PDE4B sequence was “CCUGCAAGAAGAAUC AUAU”. The si-Nrf2 sequence was “CCGAAUUACAGU GUCUUAATT”. The si-GPX4 sequence was “GCUGCG UGGUGAAGCGCUATT”. siRNA and P3000™ reagent were mixed in opti-MEM, while the Lipofectamine™ 3000 was mixed with opti-MEM in another tube. After incubation

at room temperature for 5 min. These two were mixed gently, incubated at room temperature for 20 min, and added to the cells. Subsequent experiments were conducted after incubation for 24 h.

Detection of MDA Levels

HT-22 cells were seeded at a density of 80–90%. The next day, the cells were pretreated with Roflu (1 μM) for 1 h and washed with PBS. Then, the medium was changed to glucose-free DMEM. The cells were exposed to OGD/R and rapidly stored at − 80ºC. The next day, the cells were lysed on ice and the lysate was centrifuged at 12 000 r/min for 5 min at 4ºC. Then, the supernatant was collected for MDA assay, and the optical density at 532 nm was measured by a microplate reader. Finally, the protein concentration in samples was determined by the bicinchoninic acid (BCA) method, and MDA values were normalized by protein concentrations.

Determination of Intracellular Lipid ROS Levels

The intracellular lipid ROS levels were determined by the Image-iTTM Lipid Peroxidation Kit, which is based on the oxidation–reduction of BODIPY C11 [23]. HT-22 cells were seeded at a density of 60–70%. After exposure to OGD/R, the cells were incubated with BODIPY C11 away from light for 30 min. The cells were washed with PBS once. Finally, the medium was replaced with DMEM and the cells were imaged by confocal microscopy.

Detection of Intracellular Lipid Peroxidation

HT-22 cells were seeded at a density of 70–80%. The next day, cells were incubated with 50 μM Click-iTTM LAA and then exposed to OGD/R. The cells were washed three times with PBS and then immediately fixed with 4% paraformaldehyde immediately for 15 min. Next, the cells were incubated with 0.5% Triton X-100 for 10 min and blocked with 1% bovine serum albumin for 30 min. The cells were washed three times with PBS and incubated with a Click-iTTM reaction cocktail away from light for 30 min. Finally, the cells were washed once with 1% bovine serum albumin and twice with PBS and imaged using confocal microscopy. Fluorescence intensity was analyzed by ImageJ software.

Mitochondrial Membrane Potential Measurement

The mitochondrial membrane potential (MMP) was measured by TMRE staining [24]. HT-22 cells were seeded at a density of 70–80%. The next day, the cells were exposed to OGD/R. Then, the cells were washed with PBS. The TMRE (50 nM) dye was added to the dishes, which were incubated away from light for 15 min. The cells were washed with PBS twice and the cells were imaged by confocal microscopy. Quantitative analysis was performed using ImageJ.

Transmission Electron Microscopy

HT-22 cells were seeded in six-well plates. The next day, the cells were pretreated with 1 μM Roflu. After the cells were exposed to OGD/R, they were scraped off gently. The cells were collected by centrifugation (1500 r/min) for 5 min, and immediately infiltrated by glutaraldehyde. The cells were fixed at room temperature for 1 h, and stored at 4ºC overnight. The next day, the cells were carefully washed with precooled PBS three times. The cells were sliced into ultrathin sections and imaged using a transmission electron microscope [24].

Determination of Intracellular Fe^{2+} Levels

Intracellular Fe^{2+} levels were determined by FerroOrange staining [25]. HT-22 cells were seeded at a density of 60–70%. After the cells were exposed to OGD/R, the medium was changed to DMEM containing 1 μM FerroOrange, and the cells were incubated away from light in a 37ºC thermotank for 30 min. Finally, the free Fe^{2+} levels were determined by confocal microscopy. Quantitative analysis was performed using ImageJ.

Detection of Intracellular GSH Level

The GSH level was detected using a GSH test kit according to the manufacturer's instructions. HT-22 cells were seeded in 12-well plates at a density of 60–70%. After the cells were exposed to OGD/R, PBS was added to each well and scraped off the cells gently. The cells were then broken up by sonication. The supernatant was collected after centrifuging at 12,000 r/min for 20 min. The GSH level in the supernatant was detected according to the method provided by the manufacturer. The protein level in the supernatant was detected using the BCA method. Finally, the GSH levels in individual samples were calibrated using protein concentrations.

Rotarod Test

The rotarod test was conducted 72 h after MCAO surgery [9, 26]. First, the rats were placed on a rotating drum (#YLS-31A, Yiyan S&T Development Co., Ltd., Jinan, Shandong, China), and then the speed of the rotating drum was increased from 3 to 30 rpm in 60 s. The time the rats stayed on the rod was recorded. The rats were trained three times a day for three days before MCAO surgery until they could stay on the rod for at least 60 s.

Adhesive-removal Test

The adhesive removal test was performed as previously described [9]. An adhesive tape (3 cm × 1 cm) was wrapped around the unaffected forepaw. The time it took for the rats to remove the tape (latency to remove) was recorded up to 90 s. The rats were trained once a day for three days before MCAO surgery.

Western Blot

Cells or tissues were lysed in RIPA buffer (#FD009, Fude Biological Technology, Hangzhou, China) containing 1% protease inhibitor, followed by ultrasonication and centrifugation. The supernatant was collected and the protein concentration was determined using a BCA Protein Assay Kit (#A53225, Thermo Fisher Scientific). After adjusting the concentration of each sample, the samples were boiled at 98 °C for 12 min. The proteins were separated by SDS-PAGE and transferred to PVDF membranes (#ISEQ00010, Merck), which were blocked in 5% skim milk and incubated with primary antibody at 4 °C overnight. The next day, the membranes were washed, incubated with a secondary antibody at room temperature for 1–2 h, and washed again. Finally, the protein bands were visualized and imaged using an imaging system.

Statistical Analysis

All data are expressed as mean ± standard deviation (mean ± SD). Comparisons between the two groups were analyzed by Student's unpaired *t*-test. Comparisons between three or more groups were analyzed by one-way analysis of variance followed by Tukey's post hoc test. The histograms were generated by GraphPad Prism 8.0. $P < 0.05$ was considered to indicate statistical significance.

Results

Overexpression of PDE4B Enhances Fe^{2+} Levels and Cell Death in HT-22 Cells Exposed to OGD/R

To investigate which types of cell death were involved in the OGD/R-induced neuronal cell damage, HT-22 cells were pretreated with z-VAD-FMK (Zvad, a pan-caspase inhibitor), necrostatin-1 (Nec-1, an inhibitor of necroptosis), chloroquine (CQ, a lysosome inhibitor), deferoxamine (DFO, an iron-chelating agent), and ferrostatin-1 (Fer-1, a ferroptosis inhibitor), followed by OGD/R treatment, after which the cell viability was examined using a CCK-8 assay. We found that treatment with nearly all of the inhibitors increased the viability of HT-22 cells (Fig. S1). These data indicate that multiple types of cell death contribute to OGD/R-induced cell injury. We also found that the cell survival rate was reversed by both DFO and Fer-1. These results suggest that ferroptosis is essentially involved in OGD/R-induced neuronal damage. To further verify the involvement of ferroptosis in the cell death induced by OGD/R, HT-22 cells were treated with the ferroptosis inhibitor Fer-1 before OGD/R. We found that OGD/R decreased cell viability significantly ($P < 0.01$), while Fer-1 blocked the effects of OGD/R and enhanced the viability of HT-22 cells ($P < 0.01$, Fig. 1A). The PDE4B isoform is viewed as a master regulator of brain signaling and is crucial to the maintenance of brain function [27]. Our previous study also confirmed the critical role of PDE4B in the pathology of OGD/R [19]. In the present study, we investigated the protein level of PDE4B in HT-22 cells. Cells were exposed to OGD for 6 h, followed by reoxygenation for various periods of time (1–6 h). The results showed that the expression of PDE4B increased in a time-dependent manner (Fig. 1B and C). To further verify the involvement of PDE4 in OGD/R-triggered ferroptosis, FerroOrange was used to determine the Fe^{2+} content by immunofluorescence staining. As shown in Fig. 1D and E, OGD/R increased the fluorescence intensity significantly ($P < 0.001$), which indicates that the level of iron increased after OGD/R. PDE4B overexpression further increased the level of iron under OGD/R conditions ($P < 0.001$), while both Fer-1 and the iron chelator DFO reversed the effects of PDE4B overexpression and decreased the level of iron in cells subjected to OGD/R (Fig. 1D and E). Similarly, we also found that both Fer-1 ($P < 0.01$) and DFO ($P < 0.01$) blocked the inhibitory effects of PDE4B on cell viability (Fig. 1F and G). In accordance with these results, PDE4B overexpression attenuated the level of GSH under the OGD/R condition ($P < 0.001$), while Fer-1 ($P < 0.05$) and DFO ($P < 0.05$) enhanced the level of GSH in HT-22 cells subjected to OGD/R. Taken together, these results show that PDE4B overexpression enhanced the Fe^{2+} content and cell death in HT-22 cells exposed to OGD/R.

PDE4B Knockdown Attenuates OGD/R-induced Ferroptosis in HT-22 Cells

To further verify that PDE4B exacerbated ferroptosis in HT-22 cells, we knocked down PDE4B in HT-22 cells as described in our previous report [19]. The results showed that PDE4B knockdown was effective in alleviating OGD/R-induced intracellular lipid peroxidation, as evidenced by a decrease in the accumulation of oxidized BODIPY C11 in HT-22 cells (Fig. 2A and B). The role of PDE4B in lipid peroxidation was further confirmed using the Image-iT™ Lipid Peroxidation Kit. We found that PDE4B knockdown significantly reduced the fluorescence intensity in HT-22 cells ($P < 0.05$, Fig. 2C and

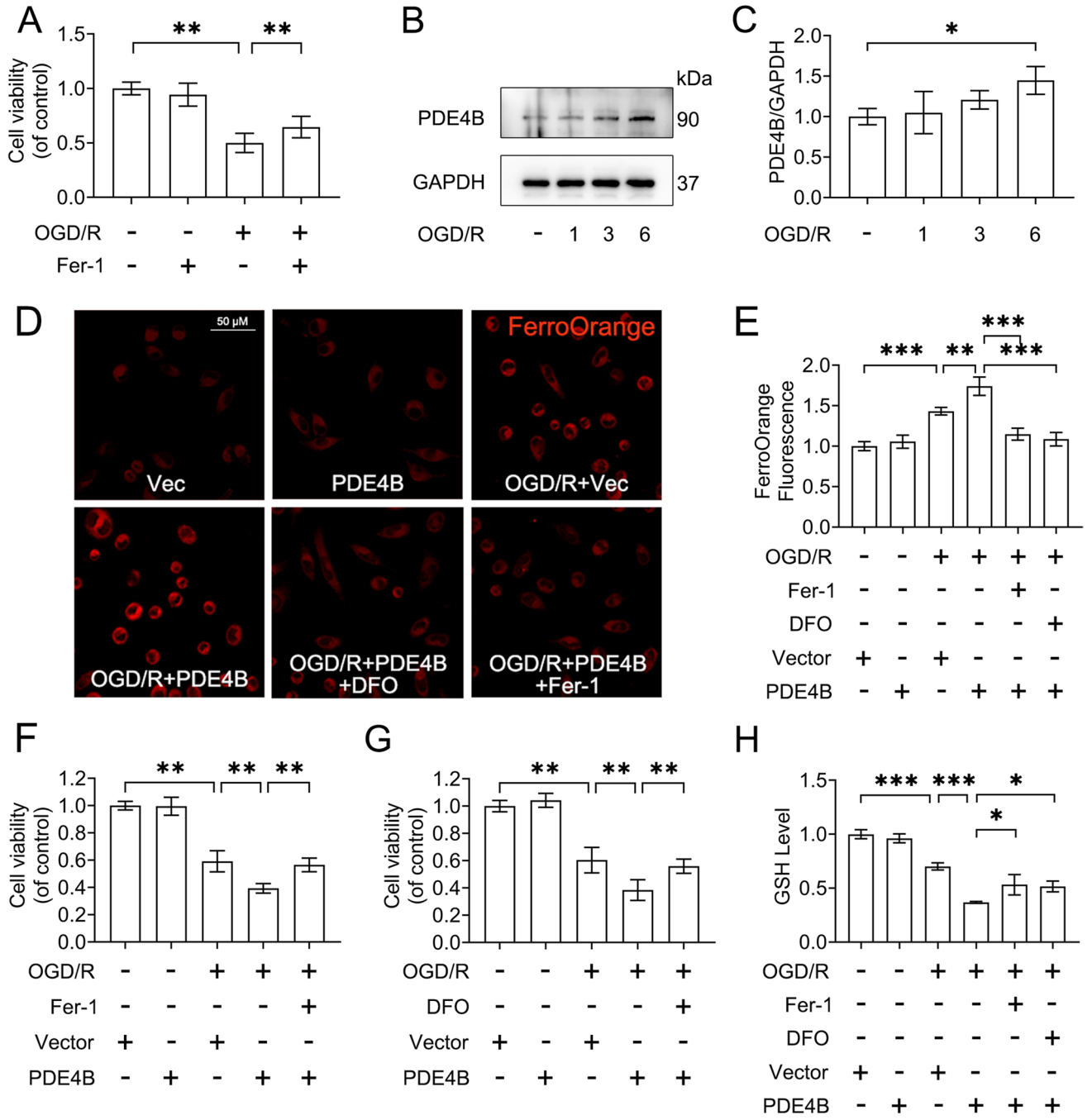

Fig. 1 Overexpression of PDE4B enhanced Fe^{2+} levels and cell death in HT-22 cells exposed to OGD/R. **A** HT-22 cells were pre-treated with Fer-1 (2 μM) for 1 h, and then cells were subjected to OGD/R. After 24 h of reoxygenation, the change in cell viability was detected using the CCK-8 assay (nine duplications from three independent experiments, n = 3). **B** HT-22 cells were subjected to OGD insult and reoxygenation for 1, 3, and 6 h. The variance of PDE4B was detected using immunoblotting. **C** Relative density analysis of PDE4B/GAPDH in HT-22 cells (n = 3). **D** HT-22 cells were transfected with a vector or a PDE4B plasmid. At 24 h after transfection, cells were incubated with Ferrostatin-1 (2 μM) or DFO (100 μM) for 1 h and then subjected to OGD/R insult. After 1 h of reoxygenation, FerroOrange staining was conducted in HT-22 cells. Scale bar: 50 μm. **E** Quantitative analysis of FerroOrange staining (n = 3). **F** After 24 h of reoxygenation, the change in cell viability was detected using the CCK-8 assay (nine duplications from three independent experiments, n = 3). **G** At 24 h after transfection, cells pretreated with DFO (100 μM) for 1 h were subjected to OGD/R insult. After 24 h of reoxygenation, the change in cell viability was detected using the CCK-8 assay (nine duplications from three independent experiments, n = 3). **H** After 1 h of reoxygenation, intracellular GSH levels were detected using a GSH detection kit (n = 3). Data are presented as mean ± SD values. $^{*}P < 0.05$, $^{**}P < 0.01$, and $^{***}P < 0.001$ versus the indicated group

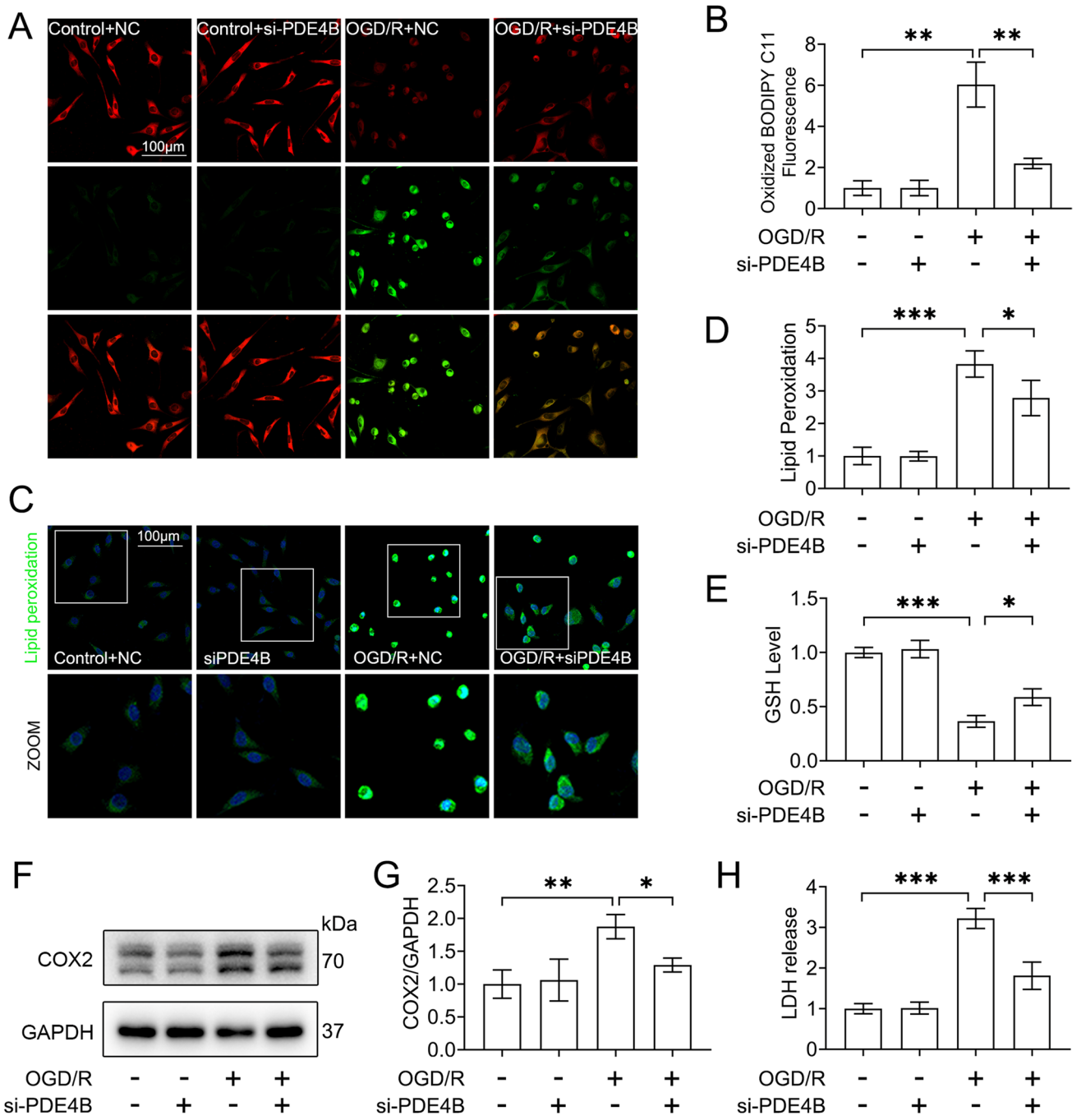

Fig. 2 PDE4B knockdown attenuated OGD/R-induced lipid peroxidation in HT-22 cells. HT-22 cells were transfected with NC or si-PDE4B. At 24 h after transfection, cells were subjected to OGD/R insult. **A** After 1 h of reoxygenation, intracellular lipid ROS levels were examined using BODIPY staining. Red represents reduced BODIPY-C11; and green represents oxidized BODIPY-C11. Scale bar: 100 μm. **B** Quantitative analysis of oxidized BODIPY C11 staining (n = 4). **C** After 1 h of reoxygenation, a Click-iTTM Lipid Peroxidation Imaging Kit was used to detect the level of intracellular lipid peroxidation. Scale bar: 100 μm. **D** Quantitative analysis of lipid peroxidation staining (n = 3). **E** After 1 h of reoxygenation, intracellular GSH levels in HT-22 cells were detected using a GSH detection kit (n = 3). **F** The variance of COX2 was detected using immunoblotting. **G** Relative density analysis of COX2/GAPDH in HT-22 cells (n = 4). **H** The LDH release was detected using an LDH cytotoxicity assay kit (n = 3). Data are presented as mean ± SD values. $^{*}P < 0.05$, $^{**}P < 0.01$, and $^{***}P < 0.001$ versus the indicated group

D). Consistent with the decrease in lipid peroxidation, the level of GSH increased in cells subjected to OGD/R and treated with PDE4B siRNA ($P < 0.05$, Fig. 2E). We then found that PDE4B knockdown was able to alleviate the release of LDH ($P < 0.001$) and the upregulation of COX2 ($P < 0.05$, Fig. 2F–H), a ferroptosis marker protein.

Meanwhile, we also found that PDE4B knockdown reduced the level of Fe^{2+} in HT-22 cells subjected to OGD/R ($P < 0.05$, Fig. 3A and B). We then investigated iron-related proteins. We found that PDE4B knockdown alleviated the downregulation of FPN ($P < 0.001$, Fig. 3C and F) and FTH1 ($P < 0.01$, Fig. 3D and G). Interestingly, the level of NCOA4 decreased ($P < 0.05$, Fig. 3E and H). The above results indicated that PDE4B knockdown alleviated OGD/R-induced ferroptosis.

Inhibition of PDE4 Ameliorates OGD/R-induced Lipid Peroxidation in HT-22 Cells

We then examined the effect of PDE4 inhibition by Roflu on ferroptosis in HT-22 cells after OGD/R treatment. Cells pretreated with Roflu were subjected to OGD for 6 h and oxygenation for various periods of time (3–24 h). As shown in Fig. 4A, Roflu decreased the release of LDH in HT-22 cells after oxygenation for 12 or 24 h. We then investigated the changes in intracellular lipid peroxidation by measuring GSH and MDA levels (Fig. 4B and C). Compared with the control group, OGD/R-induced cells exhibited an increase in the MDA level ($P < 0.01$) but a decrease in the GSH level ($P < 0.01$). Treatment of HT-22 cells with Roflu decreased the level of MDA ($P < 0.05$) and enhanced the level of GSH ($P < 0.05$). Furthermore, we found that Roflu decreased COX2 expression ($P < 0.01$, Fig. 4D and E). We then determined the intracellular lipid peroxidation levels using two

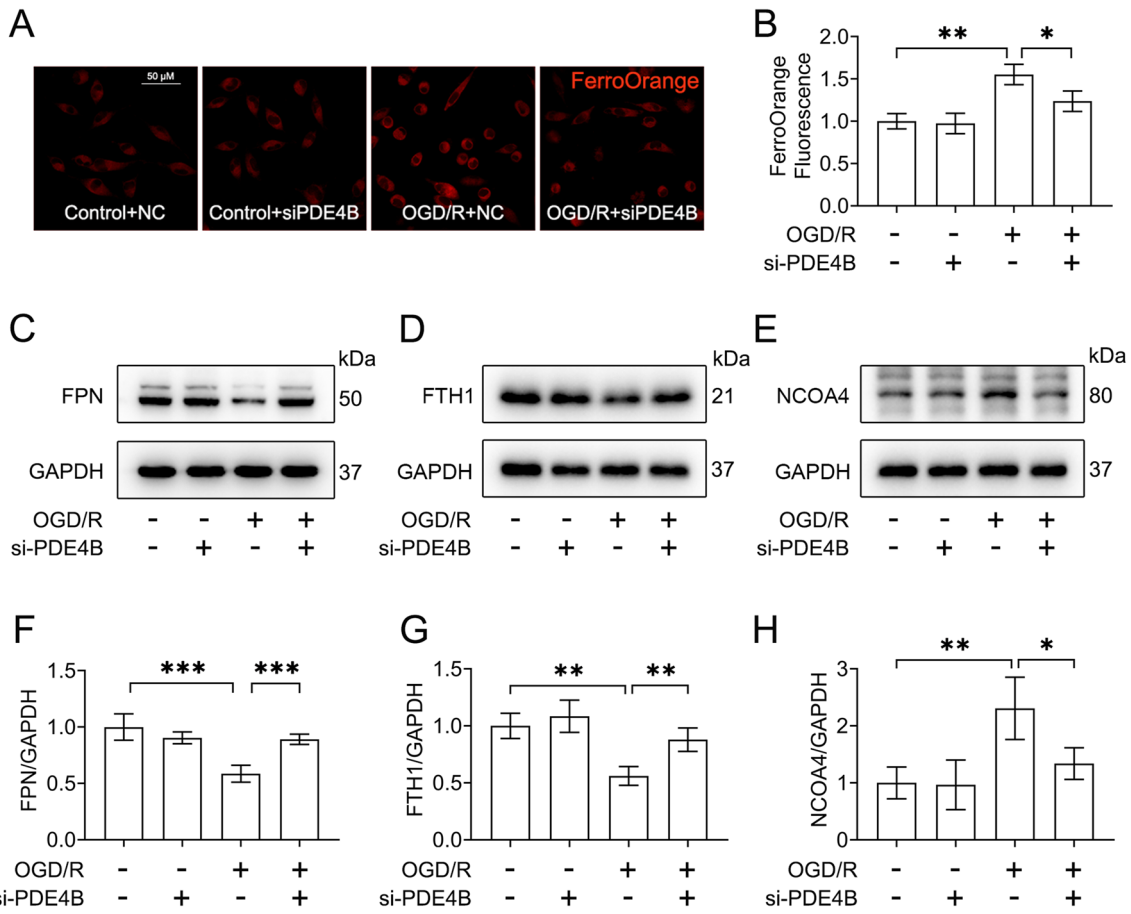

Fig. 3 PDE4B knockdown attenuated OGD/R-induced accumulation of Fe^{2+} in HT-22 cells. HT-22 cells were transfected with NC or si-PDE4B. At 24 h after transfection, cells were subjected to OGD/R insult. **A** After 1 h of reoxygenation, FerroOrange staining was conducted in HT-22 cells. Scale bar: 50 μm. **B** Quantitative analysis of FerroOrange staining (n = 3). **C**-**E** After 1 h of reoxygenation, the variances of FPN, FTH1, and NCOA4 were detected using immunoblotting. **F**–**H** Relative density analysis of FPN/GAPDH (n = 4), FTH1/GAPDH (n = 4), NCOA4/GAPDH (n = 4) in HT-22 cells. Data are presented as mean ± SD values, $^{*}P < 0.05$, $^{**}P < 0.01$, and $^{***}P < 0.001$ versus the indicated group

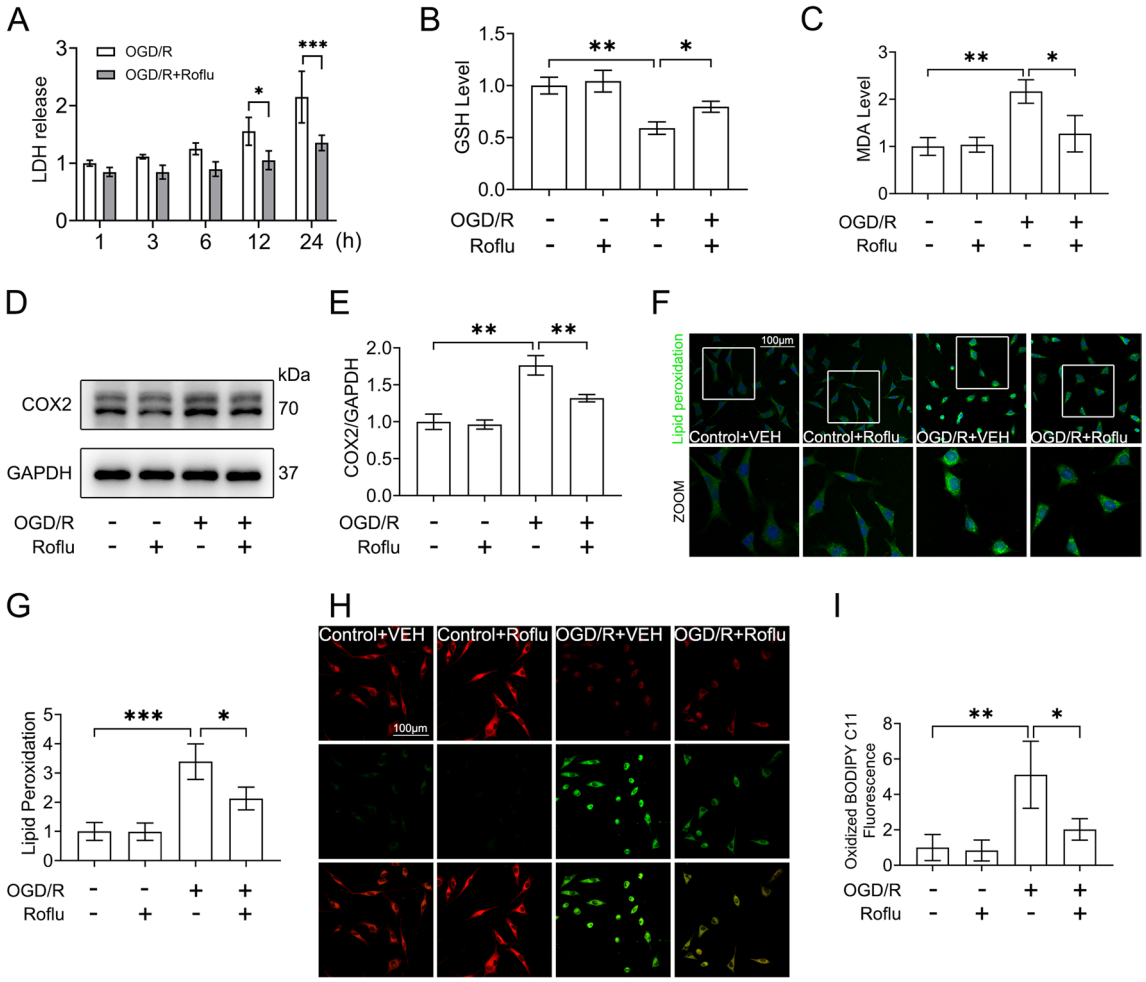

Fig. 4 Inhibition of PDE4 ameliorated OGD/R-induced lipid peroxidation in HT-22 cells. **A** HT-22 cells were subjected to OGD insult. After 1, 3, 6, 12, and 24 h of reoxygenation, the LDH release was detected using an LDH Cytotoxicity Assay Kit (n = 3). **B** HT-22 cells were pre-incubated with Roflu (1 μM) for 1 h, and then cells were subjected to OGD/R. After 1 h of reoxygenation, intracellular GSH levels were detected using a GSH detection kit (n = 3). **C** After 1 h of reoxygenation, intracellular MDA levels were detected using an MDA detection kit (n = 3). **D** After 1 h of reoxygenation, the variance of COX2 was detected by immunoblotting. **E** Relative density analysis of COX2/GAPDH in HT-22 cells (n = 3). **F** After 1 h of reoxygenation, a Click-iTTM Lipid Peroxidation Imaging Kit was used to detect the level of intracellular lipid peroxidation. Scale bar: 100 μm. **G** Quantitative analysis of lipid peroxidation staining (n = 3). **H** After 1 h of reoxygenation, intracellular lipid ROS levels were examined using BODIPY staining. Scale bar: 100 μm. **I** Quantitative analysis of oxidized BODIPY C11 staining (n = 3). Data are presented as mean ± SD values. $^{*}P < 0.05$, $^{**}P < 0.01$, and $^{***}P < 0.001$ versus the indicated group

kits, the Image-iT™ Lipid Peroxidation Kit and the Click-iTTM Lipid Peroxidation Imaging Kit. The results showed that the intracellular lipid peroxidation level significantly increased after OGD/R treatment, and Roflu was able to effectively alleviate OGD/R-induced lipid peroxidation in HT-22 cells (Fig. 4F–I).

At the same time, TMRE was used to quantify the MMP. We found that OGD/R triggered a decrease in MMP ($P < 0.001$), while treatment with Roflu (0.1–1 μM) increased the MMP in a concentration-dependent manner (Fig. 5A and B). We also used transmission electron microscopy to observe the changes in mitochondrial morphology in HT-22 cells after OGD/R treatment. We found that the mitochondria in HT-22 cells were obviously sequestered after OGD/R treatment, and Roflu was able to effectively reduce the sequestration of mitochondria (Fig. 5C). The above results indicate that inhibition of PDE4 could alleviate OGD/R-induced ferroptosis in HT-22 cells.

Inhibition of PDE4 Alleviates OGD/R-induced Accumulation of Fe^{2+} in HT-22 Cells

Ferroptosis is an iron-dependent form of programmed cell death. Therefore, we next examined the changes in intracellular free Fe^{2+} levels using FerroOrange staining. The experimental results showed that intracellular free Fe^{2+}

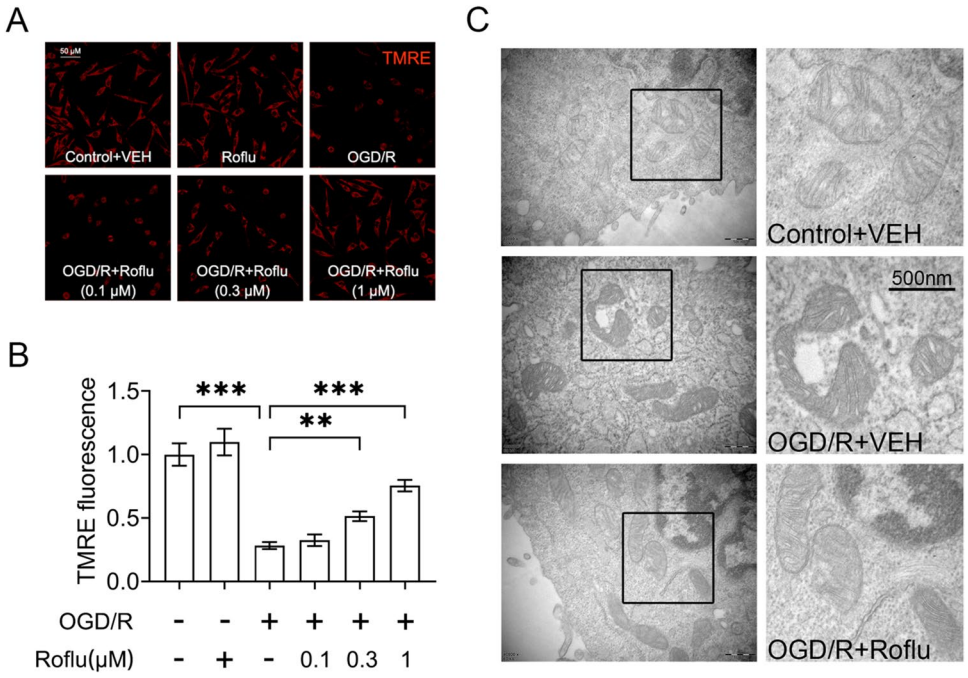

Fig. 5 Inhibition of PDE4 alleviated OGD/R-induced mitochondrial membrane potential loss and mitochondrial pyknosis in HT-22 cells. **A**-**B** HT-22 cells were pre-incubated with Roflu (1 μM) for 1 h, and then cells were subjected to OGD/R. After 1 h of reoxygenation, MMP was visualized using TMRE staining, and statistical analyses were conducted using ImageJ (n = 3). Scale bar: 50 μm. **C** The changes in the mitochondrial morphology were observed using transmission electron microscopy. Scale bar: 500 nm. Data are presented as mean ± SD values. $^{**}P < 0.01$ and $^{***}P < 0.001$ versus the indicated group

levels increased after OGD/R treatment ($P < 0.01$), and Roflu was able to alleviate intracellular free Fe^{2+} accumulation ($P < 0.01$, Fig. 6A and B). Ferritin is an important protein in the intracellular regulation of free iron levels, and changes in the levels of FTH1, the heavy chain of intracellular ferritin, reflect changes in the levels of intracellular ferritin [28]. We therefore examined the changes in FTH1 protein levels. We found that intracellular FTH1 expression was significantly reduced after OGD/R treatment ($P < 0.01$), and Roflu was able to effectively alleviate the OGD/R-induced reduction in FTH1 levels ($P < 0.01$, Fig. 6C, E). By contrast, ferritinophagy during ischemic brain injury can lead to intracellular Fe^{2+} accumulation by degrading ferritin, which in turn aggravates ferroptosis [29]. Therefore, we examined the changes in the levels of NCOA4, a key protein in ferritinophagy [30]. The results showed that NCOA4 expression was significantly upregulated in HT-22 cells after OGD/R treatment ($P < 0.01$), and Roflu was able to alleviate the OGD/R-induced upregulation of NCOA4 ($P < 0.05$, Fig. 6C and D). FPN, an iron exporter in mammals, plays a critical role in iron homeostasis [31]. We found that the level of FPN decreased in HT-22 cells after OGD/R ($P < 0.01$), whereas Roflu restored the level of FPN ($P < 0.001$, Fig. 6F and G).

To further verify the protective effects of Roflu against ferroptosis, HT-22 cells were treated with the ferroptosis inducers erastin and RSL3. The results showed that erastin (2.5–20 μM) and RSL3 (1.25–10 μM) reduced cell viability in a concentration-dependent manner (Fig. 7A and B), whereas Roflu (0.1–10 μM) reversed the effects of both erastin and RSL3 (Fig. 7C and D). Taken together, these data indicate that inhibition of PDE4 is beneficial to iron homeostasis in neuronal cells under OGD/R conditions.

Knockdown of GPX4 Blocks the Protective Effect of Roflu Against OGD/R-induced Ferroptosis in HT-22 Cells

In the present study, Roflu was found to enhance the level of GSH. Glutathione peroxidase 4 (GPX4) is an enzyme that reduces lipid peroxidation of cell membranes using GSH as a co-factor [32]. We then further investigated whether GPX4 mediates the protective effects of Roflu against ferroptosis in neuronal cells. GPX4 was knocked down in HT-22 cells (Fig. 8A and B). Roflu inhibited the OGD/R-induced reduction in cell viability ($P < 0.01$), while knockdown of GPX4 blocked this effect and decreased the viability of HT-22 cells ($P < 0.01$, Fig. 8C). We also found that Roflu enhanced the viability of primary cultured neurons under the OGD/R condition, and knockdown of GPX4 by siRNA blocked the protective effects of Roflu in neurons (Fig. S2). Consistent with these results, Roflu effectively alleviated OGD/R-induced intracellular lipid ROS accumulation, as evidenced by increased levels of the oxidized state of BODIPY C11 (green in Fig. 8D and E) and the fluorescence intensity of lipid peroxidation (Fig. 8F and G), whereas knockdown of GPX4 blocked the effect of Roflu on intracellular lipid ROS levels (Fig. 8D–G). These results suggest that GPX4 is involved in the protective effects of Roflu against OGD/R-induced ferroptosis.

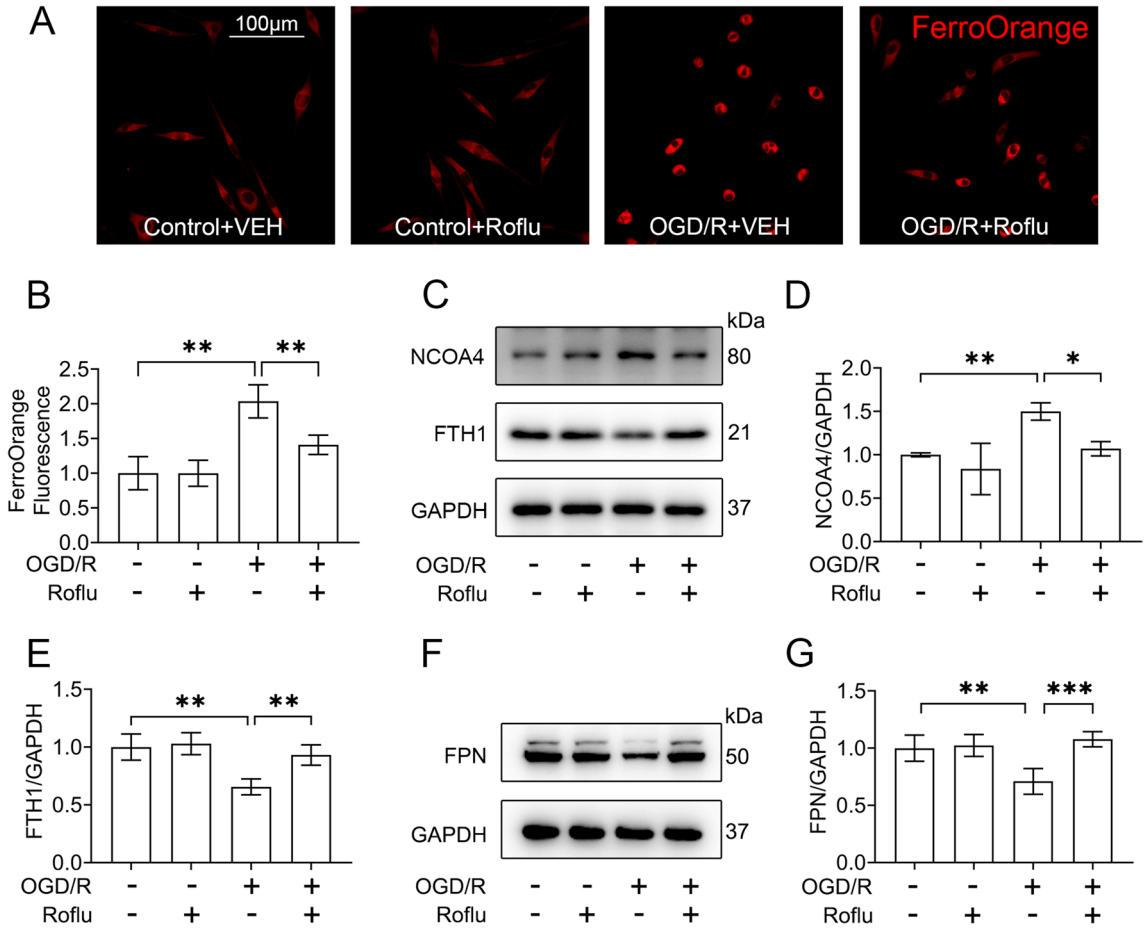

Fig. 6 Inhibition of PDE4 alleviated OGD/R-induced accumulation of Fe^{2+} in HT-22 cells. HT-22 cells were pre-incubated with Roflu (1 μM) for 1 h, and then cells were subjected to OGD/R. **A** After 1 h of reoxygenation, FerroOrange staining was conducted in HT-22 cells. Scale bar: 50 μm. **B** Quantitative analysis of FerroOrange staining (n = 4). **C** After 1 h of reoxygenation, the variance of FTH1 and NCOA4 were detected by immunoblotting. **D**-**E** Relative density analysis of FTH1/GAPDH (n = 3), NCOA4/GAPDH (n = 3) in HT-22 cells. **F** After 1 h of reoxygenation, the variance of FPN was detected by immunoblotting. **G** Relative density analysis of FPN/GAPDH in HT-22 cells (n = 5). Data are presented as mean ± SD values. $^{*}P < 0.05$, $^{**}P < 0.01$, and $^{***}P < 0.001$ versus the indicated group

Knockdown of Nrf-2 Blocks the Protective Effect of PDE4 Inhibition Against OGD/R-induced Ferroptosis

Having clarified the involvement of GPX4 in the protective effect of PDE4 inhibition, we next examined the mechanism by which inhibition of PDE4 promotes GPX4 expression. In our previous study, we found that inhibition of PDE4 promoted OGD/R-induced Nrf-2 expression [19], and it was shown that Nrf-2 upregulated GPX4 expression [33]. In ischemic brain injury, the relationship between Nrf-2 and GPX4 is unclear. Therefore, we next examined the role of Nrf-2 in the regulation of GPX4 under OGD/R conditions. Nrf-2 was knocked down in HT-22 cells (Fig. 9A and B). We then examined the effects of Nrf-2 knockdown on the release of LDH. We found that Roflu decreased the release of LDH ($P < 0.05$, Fig. 9C), while Nrf-2 knockdown blocked the effects of Roflu and increased the release of LDH ($P < 0.05$, Fig. 9C). We then found that Roflu decreased Fe^{2+} accumulation and Nrf-2 knockdown increased Fe^{2+} accumulation ($P < 0.05$, Fig. 9D and E). Similarly, Nrf-2 knockdown reduced the level of FPN in Roflu-treated cells ($P < 0.01$, Fig. 9F and G).

We also investigated the effects of Nrf-2 knockdown on lipid peroxidation. The results showed that the knockdown of Nrf-2 resulted in decreased GSH levels ($P < 0.01$, Fig. 10A). We then examined the effect of Nrf-2 knockdown on GPX4 levels under OGD/R conditions. Consistent with the previous results, Roflu promoted GPX4 expression ($P < 0.05$, Fig. 10B and C). While Nrf-2 knockdown downregulated GPX4 expression, it also blocked the effect of Roflu on GPX4 expression ($P < 0.01$, Fig. 10B and C). We also found that Nrf-2 knockdown led to more intracellular accumulation of lipid ROS, and Roflu downregulated

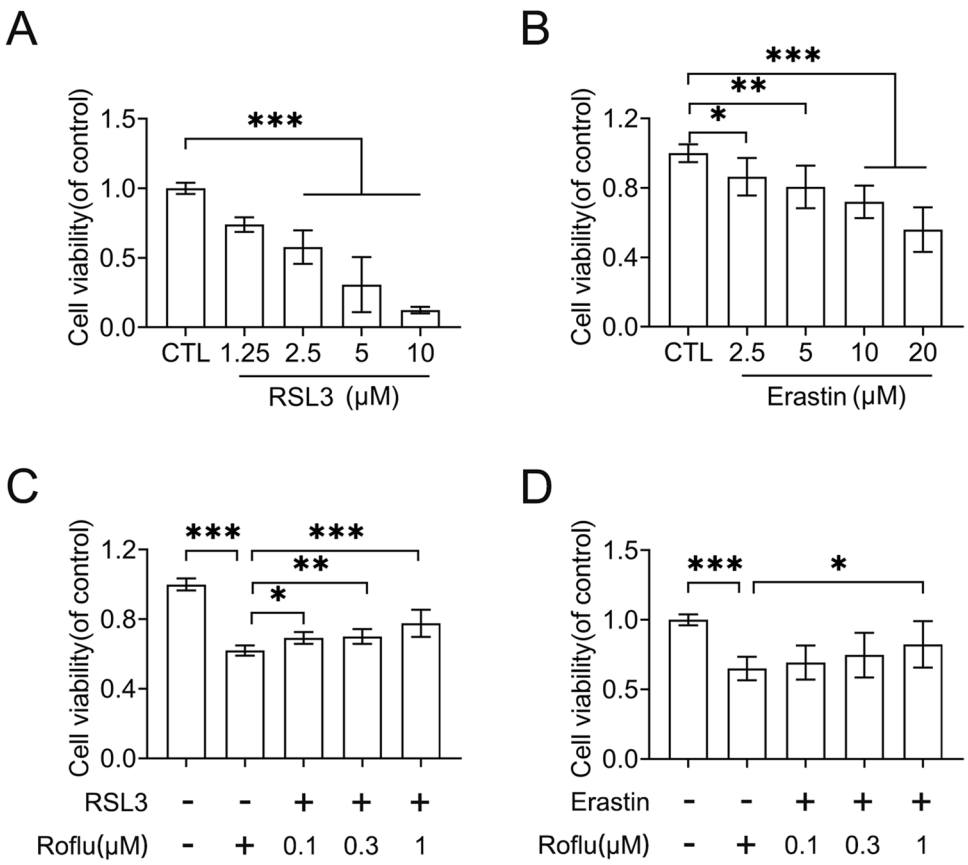

Fig. 7 Inhibition of PDE4 alleviated ferroptosis induced by RSL3 or Erastin. **A**-**B** HT-22 cells were treated with RSL3 (1.25, 2.5, 5, and 10 μM) or Erastin (2.5, 5, 10, and 20 μM) to induce ferroptosis. After 24 h, the change in cell viability was detected using a CCK-8 assay (nine duplications from three independent experiments, n = 3). **C**-**D** HT-22 cells were pretreated with Roflu (0.1, 0.3, 1 μM) for 1 h and subjected to RSL3 (5 μM) or Erastin (20 μM) treatment. After 24 h, the change in cell viability was detected using the CCK-8 assay (nine duplications from three independent experiments, n = 3). Data are presented as mean ± SD values. $^{*}P < 0.05$, $^{**}P < 0.01$, and $^{***}P < 0.001$ versus the indicated group

intracellular lipid ROS levels ($P < 0.01$). Importantly, Nrf-2 knockdown blocked the effects of Roflu ($P < 0.01$, Fig. 10D and E). These results indicate that inhibition of PDE4 alleviated OGD/R-induced ferroptosis by enhancing Nrf-2/GPX4.

Inhibition of PDE4 Alleviates MCAO/R-induced Ferroptosis

Our above results revealed the effects of PDE4 inhibition on ferroptosis in HT-22 cells. Next, we examined the protective role of Roflu in an animal model of MCAO/R. Consistent with the results obtained in the cellular experiments, we found that the level of iron was elevated in the brain tissue of rats following MCAO/R injury, and the inhibition of PDE4 reduced the level of iron (Fig. S3). RSL3, a GPX4 inhibitor, was used to further demonstrate the modulatory effect of Roflu on ferroptosis. The volume of cerebral infarction in Sprague–Dawley rats was determined using TTC staining. We found that Roflu reduced the cerebral infarct volume ($P < 0.01$), whereas RSL3 blocked the effect of Roflu on cerebral infarction ($P < 0.01$, Fig. 11A and B). Next, the neurological deficit scores were evaluated. Consistent with the above results, Roflu was able to reduce the neurological deficit scores ($P < 0.01$), and RSL3 blocked the protective effect of Roflu ($P < 0.01$, Fig. 11C). To determine the functional significance of the neuroprotective effects of Roflu, a rotarod test and an adhesive-removal test were conducted to evaluate the sensorimotor deficits in rats. We found that inhibition of PDE4 significantly ameliorated behavioral deficits in animals after cerebral ischemia (Fig. 11D and E). We then detected oxidative stress occurring in the ischemic penumbra of rats following MCAO/R. Our results demonstrated that Roflu significantly increased GSH ($P < 0.001$) and decreased MDA ($P < 0.01$) levels. When GPX4 was inhibited by RSL3, Roflu failed to rescue the content of GSH ($P < 0.001$), and the level of MDA ($P < 0.01$) increased as well (Fig. 11F and G). ACSL4, COX2, and FPN were selected as representative ferroptosis indicators. The results showed that ACSL4 ($P < 0.001$) and COX2 ($P < 0.001$) were significantly upregulated in the ischemic penumbra of rats after MCAO/R, while the level of FPN decreased ($P < 0.01$). Treatment with Roflu significantly reduced the expression of ACSL4 ($P < 0.001$) and COX2 ($P < 0.01$) (Fig. 11H–J). Roflu also enhanced the level of FPN (Fig. 11H and K, $P < 0.01$). Interestingly, RSL3 blocked the protective effects of Roflu. The levels of ACSL4 ($P < 0.01$) and COX2 ($P < 0.05$) increased, whereas the FPN ($P < 0.001$) level decreased after application of RSL3 (Fig. 11H–K). The

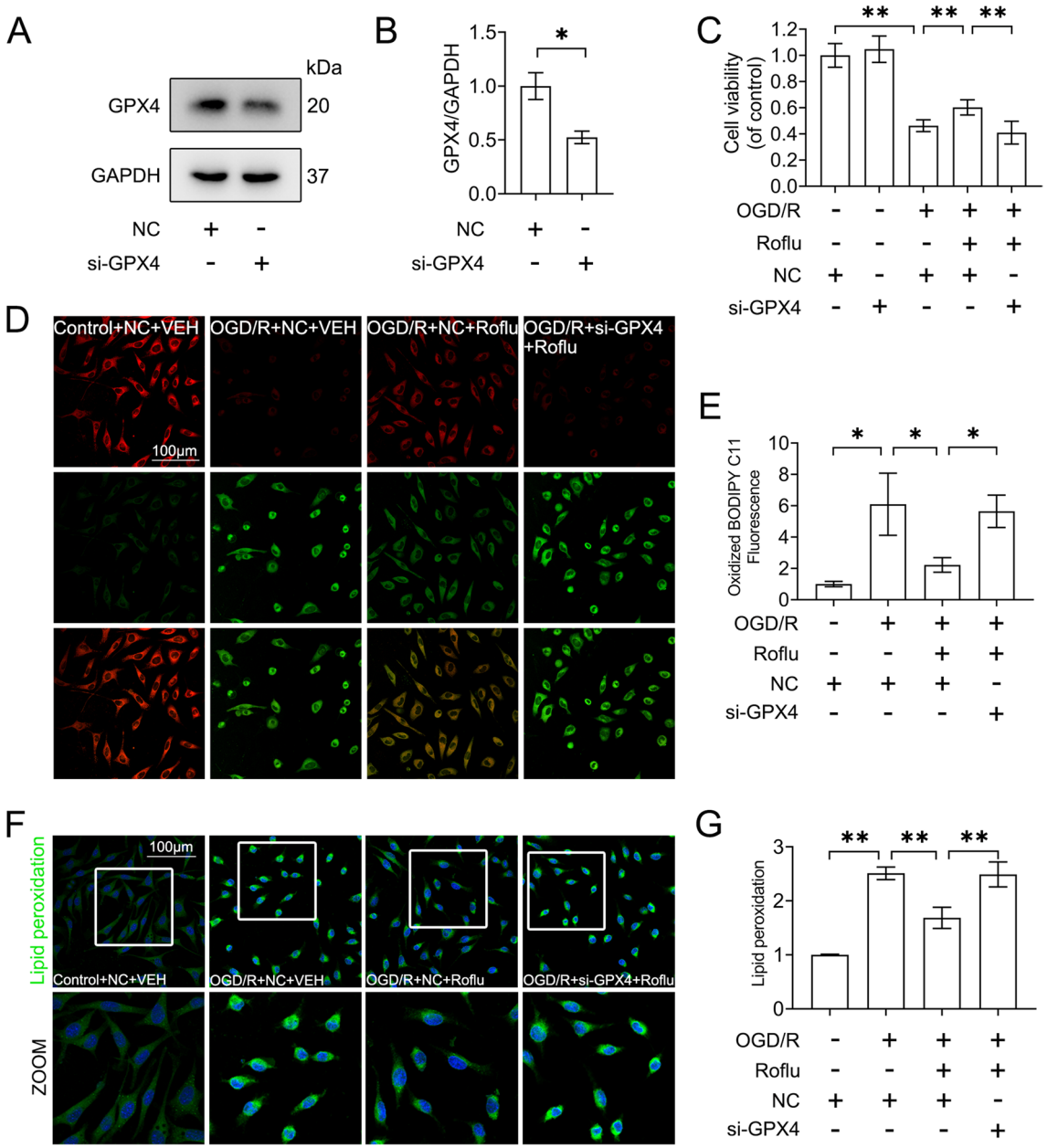

Fig. 8 Knockdown of GPX4 blocked the protective effect of Roflu against OGD/R-induced ferroptosis in HT-22 cells. **A** HT-22 cells were transfected with NC or si-GPX4 for 24 h. The variance of GPX4 was detected using immunoblotting. **B** Relative density analysis of GPX4/GAPDH in HT-22 cells (n = 3). **C** HT-22 cells were transfected with NC or si-GPX4. At 24 h after transfection, cells were incubated with Roflu (1 μM) for 1 h and then subjected to OGD/R insult. After 24 h of reoxygenation, cell viability was detected using the CCK-8 assay (nine duplications from three independent experiments, n = 3). **D** After 1 h of reoxygenation, intracellular lipid ROS levels were examined using BODIPY staining. Scale bar: 100 μm. **E** Quantitative analysis of oxidized BODIPY C11 staining (n = 3). **F** After 1 h of reoxygenation, a Click-iTTM Lipid Peroxidation Imaging Kit was used to detect the level of intracellular lipid peroxidation. Scale bar: 100 μm. **G** Quantitative analysis of lipid peroxidation staining (n = 3). Data are presented as mean ± SD values. $^{*}P < 0.05$ and $^{**}P < 0.01$ versus the indicated group

above results indicated that MCAO/R induced ferroptosis in the ischemic penumbra of Sprague–Dawley rats, and inhibition of PDE4 significantly alleviated the MCAO/R-induced ferroptosis.

Discussion

PDE4 is a promising target for the treatment of stroke. However, the association of PDE4 with iron-induced cell death

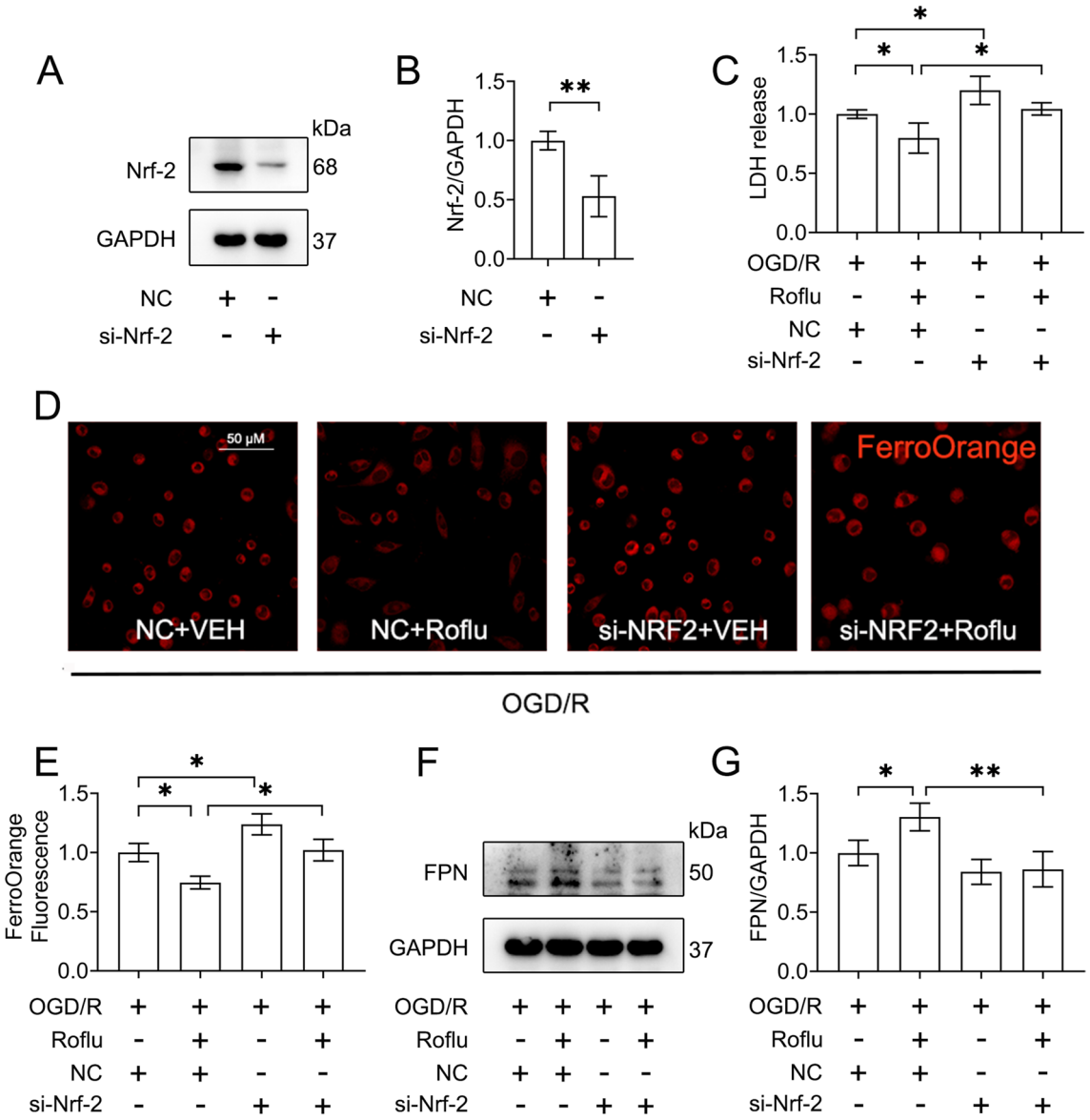

Fig. 9 Knockdown of Nrf-2 blocked the protective effect of PDE4 inhibition against OGD/R-induced accumulation of Fe^{2+}. **A** HT-22 cells were transfected with NC or si-Nrf-2 for 24 h. The variance of Nrf-2 was detected by immunoblotting. **B** Relative density analysis of Nrf-2/GAPDH in HT-22 cells (n = 4). **C** HT-22 cells were transfected with NC or si-Nrf-2. At 24 h after transfection, cells were incubated with Roflu (1 μM) for 1 h and then subjected to OGD/R insult. After 24 h of reoxygenation, the LDH release was detected using an LDH Cytotoxicity Assay Kit (n = 4). **D** After 1 h of reoxygenation, FerroOrange staining was conducted in HT-22 cells. Scale bar: 50 μm. **E** Quantitative analysis of FerroOrange staining (n = 3). **F** After 1 h of reoxygenation, the variance of FPN was detected by immunoblotting. **G** Relative density analysis of FPN/GAPDH in HT-22 cells (n = 4). Data are presented as mean ± SD values. $^{*}P < 0.05$ and $^{**}P < 0.01$ versus the indicated group

under cerebral ischemia and the signaling pathway remains only partially understood. In the present study, we explored the role of PDE4 in ferroptosis in ischemic brain injury and its possible mechanisms. We found that PDE4B overexpression enhanced lipid peroxidation, while PDE4B knockdown suppressed lipid peroxidation, reduced the accumulation of iron, and restored the expression of FTH1, FPN, and NCOA4 in HT-22 cells following OGD/R. We then found that the PDE4 inhibitor Roflu was able to alleviate OGD/R-induced intracellular lipid peroxidation and intracellular Fe^{2+} accumulation. Similarly, Roflu alleviated the OGD/R-induced increase in COX2 and NCOA4 expression and the decrease in FTH1 expression in HT-22 cells. Interestingly, further experiments revealed that GPX4 knockdown blocked the effect of Roflu on OGD/R-induced ferroptosis. Moreover, we found that the knockdown of Nrf-2 blocked the promotion of

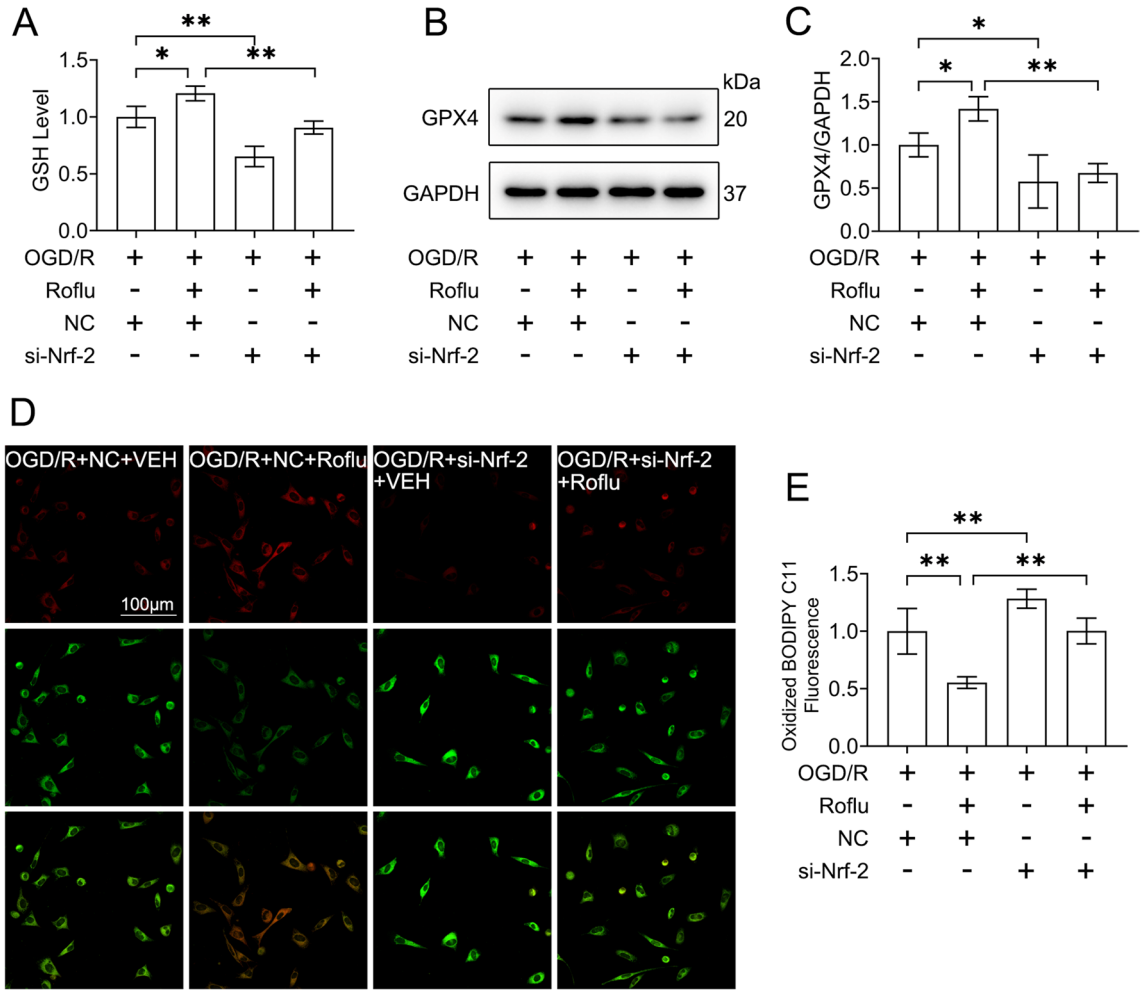

Fig. 10 Knockdown of Nrf-2 blocked the protective effect of PDE4 inhibition against OGD/R-induced lipid peroxidation. HT-22 cells were transfected with NC or si-Nrf-2. At 24 h after transfection, cells were incubated with Roflu (1 μM) for 1 h and then subjected to OGD/R insult. **A** After 1 h of reperfusion, intracellular GSH levels in HT-22 cells were detected using a GSH detection kit (n = 3). **B** After 1 h of reoxygenation, the variance of GPX4 was detected by immunoblotting. **C** Relative density analysis of GPX4/GAPDH in HT-22 cells (n = 3). **D** After 1 h of reoxygenation, intracellular lipid ROS levels were examined using BODIPY staining. Scale bar: 100 μm. **E** Quantitative analysis of oxidized BODIPY C11 staining (n = 3). Data are presented as mean ± SD values. $^{*}P < 0.05$ and $^{**}P < 0.01$ versus the indicated group

GPX4 expression by Roflu and the reduction of intracellular lipid ROS levels. This suggests that Nrf-2/GPX4 signaling mediates the role of Roflu in alleviating OGD/R-induced ferroptosis. We also verified the anti-ferroptotic effect of Roflu in an animal model of MCAO/R, and we found that RSL3, a GPX4 inhibitor, could attenuate the protective effect of Roflu. Taken together, inhibition of PDE4 alleviated ischemic brain injury-induced neuronal ferroptosis through activation of Nrf-2/GPX4. To the best of our knowledge, this study shows for the first time that inhibition of PDE4 suppresses ferroptosis under cerebral ischemia/reperfusion conditions. Our study also provides a new mechanism by which PDE4 inhibitors can ameliorate ischemic brain injury.

Excessive oxidative stress is a characteristic feature during the process of ischemic brain injury. A sudden interruption of cerebral blood flow results in cerebral damage. Reperfusion brings oxygen and glucose to neurons on the one hand but also leads to excessive ROS production [34]. ROS generation is viewed as a critical etiological factor for cerebral ischemia/reperfusion-induced neuronal injury [35]. The accumulation of ROS exacerbates mitochondrial dysfunction, endoplasmic reticulum stress, and lipid peroxidation, and may ultimately cause cell death [36]. ROS trigger cell death through multiple mechanisms, including ferroptosis, apoptosis, and autophagy [37]. Hence, inhibition of ROS production is helpful in the recovery of neurological function after cerebral ischemia/reperfusion. To protect neurons against cell death caused by stroke, it may be a promising strategy to intervene in the production or enhance the elimination of ROS. Our previous study found

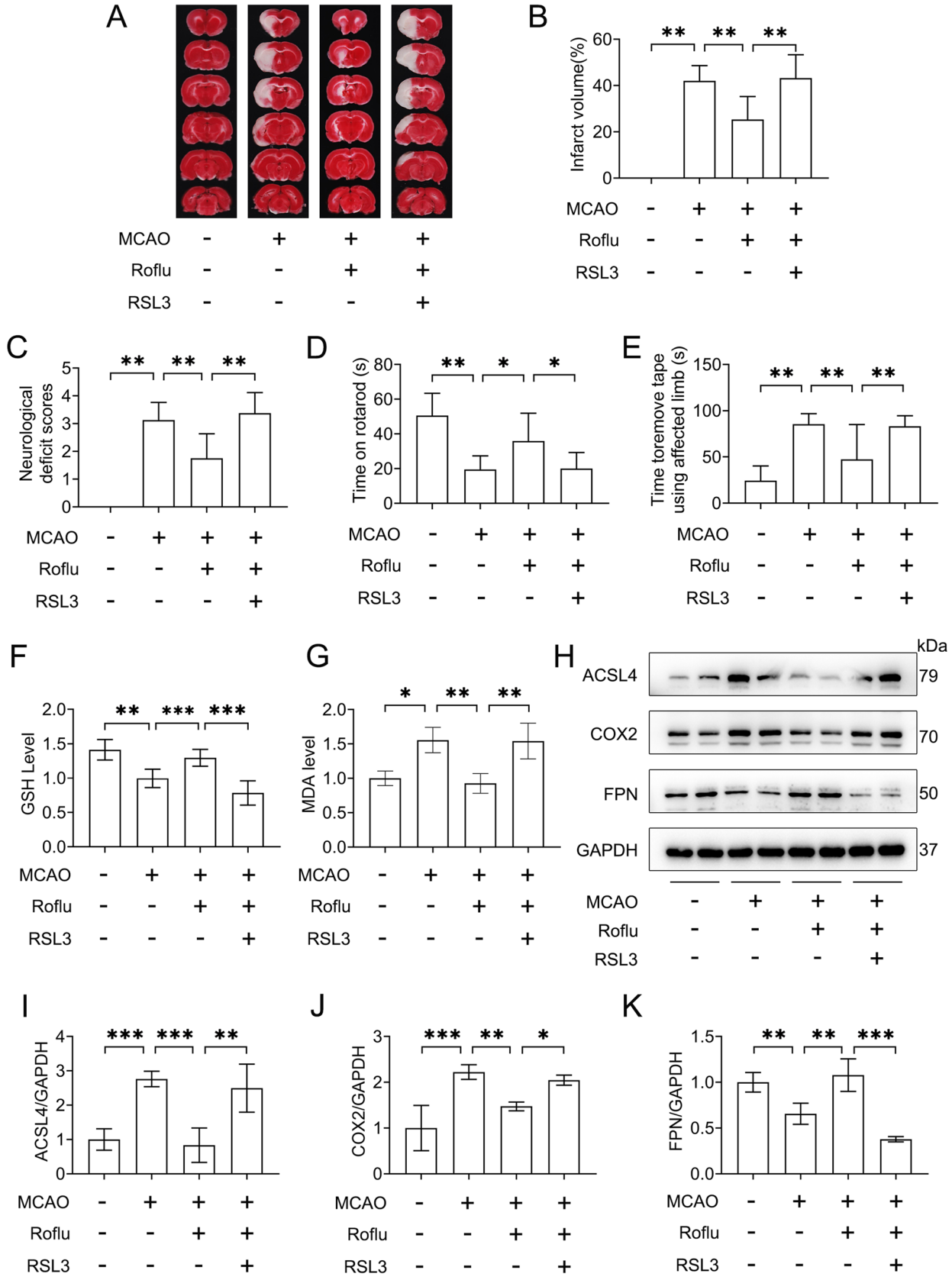
A
MCAO - + + +
Roflu - - + +
RSL3 - - - +
B
Infarct volume(%)
C
Neurological deficit scores
D
Time on rotarod (s)
E
Time toremove tape using affected limb (s)
F
GSH Level
G
MDA level
H
kDa
ACSL4
COX2
FPN
GAPDH
79
70
50
37
I
ACSL4/GAPDH
J
COX2/GAPDH
K
FPN/GAPDH

◂**Fig. 11** Inhibition of PDE4 alleviated MCAO-induced ferroptosis. SD rats were intraperitoneally injected with vehicle or RSL3 (7.5 mg/kg) at 2 h after MCAO surgery. Thirty minutes later, the vehicle or Roflu (1 mg/kg) was injected intraperitoneally. **A**–**B**After 24 h of reperfusion, the infarct volume was detected using TTC staining (n = 8). **C** After 24 h of reperfusion, the neurological deficit scores were recorded (n = 8). **D**–**E** Roflu (1.0 mg/kg), RSL3 (7.5 mg/kg), and vehicle were administered once per day for three days after surgery. A total of 72 h after MCAO reperfusion injury, a Rotarod test and adhesive-removal test were performed. The time spent on the rotarod and the time it took to remove the tape were recorded. Sham + VEH, n = 8; MCAO + VEH, n = 9; MCAO + Roflu, n = 8. MCAO + RSL3, n = 9. **F** After 24 h of reperfusion, intracellular GSH levels in the penumbra were detected using a GSH detection kit (n = 5). **G** MDA in the penumbra was detected using an MDA detection kit (n = 3). **H** After 24 h of reoxygenation, the variance of ACSL4, COX2, and FPN in the penumbra were detected by immunoblotting. **I**-**K** Relative density analysis of ACSL4/GAPDH, COX2/GAPDH, FPN/GAPDH in HT-22 cells (n = 4). Data are presented as mean ± SD values. $^{*}P < 0.05$, $^{**}P < 0.01$, and $^{***}P < 0.001$ versus the indicated group

that inhibition of PDE4 reduced the accumulation of ROS in dopaminergic neurons in Parkinson's disease [38]. We also found that inhibition of PDE4 reduced OGD/R-induced intraneuronal ROS accumulation in an ischemic brain injury model [10]. These results suggest that inhibition of PDE4 is effective in alleviating oxidative stress in neurological disorders. However, the mechanism of action by which PDE4 inhibition reduces ROS levels is not clear.

Excessive ROS production is one of the crucial events in the occurrence of ferroptosis, which is a novel form of programmed cell death characterized by iron-dependent lipid peroxidation [11]. An increasing body of evidence suggests that ferroptosis is involved in neuronal death during ischemic brain injury [18, 39, 40], and inhibition of ferroptosis is a potential strategy for the treatment of ischemic brain injury. Our previous study found that the PDE4 inhibitor FCPR03 was effective in alleviating OGD-induced accumulation of MDA and intracellular ROS in HT-22 cells [19]. In the present study, we found that the PDE4 inhibitor Roflu also reduced MDA accumulation. Based on these observations, we proposed the hypothesis that inhibition of PDE4 could alleviate ischemic brain injury-induced neuronal ferroptosis. This hypothesis was confirmed by our results. We found that knockdown or inhibition of PDE4 increased cell survival, as evidenced by an increase in cell viability and a decrease in LDH release, as well as a decrease in the level of lipid peroxidation and, more importantly, a decrease in intracellular Fe^{2+} accumulation. We confirmed these findings in an MCAO/R animal model. These data suggest that PDE4 inhibition exerts anti-ferroptotic effects in cerebral ischemia models. The mechanism whereby cerebral ischemia/reperfusion induces neuronal death is complex. Multiple cell death types may be involved. Previous studies have shown that PDE4 can participate in neuronal death after ischemic brain injury by promoting apoptosis and neuroinflammation [9, 41]. The present study confirmed that PDE4 inhibition could suppress ferroptosis. The relationships between these different types of cell death, as well as how apoptosis, neuroinflammation, and ferroptosis are related, require further study. In addition, whether other newly discovered types of programmed cell death, such as cuproptosis, are involved in the regulation of neuronal death needs to be further investigated.

Next, we are interested in how PDE4 regulates Fe^{2+} accumulation in cells subjected to ischemia. Ferritin is responsible for intracellular iron storage and can negatively regulate free Fe^{2+} levels in cells [42]. FPN is a transport protein responsible for exporting iron from cells to maintain iron homeostasis [31]. We examined the expression of FTH1 and FPN in cells. The results showed that PDE4 inhibition attenuated OGD/R-induced loss of both FPN and FTH1. Interestingly, we further found that NCOA4, a key protein mediating ferritinophagy [43], was significantly upregulated. Previous studies showed that hyperactivation of autophagy occurs during cerebral ischemia/reperfusion [17, 44]. Therefore, it is likely that FTH1 is cleared by NCOA4-mediated ferritinophagy in cells via the autophagy–lysosomal pathway. However, we have not yet examined whether PDE4 regulates ferritin autophagy through NCOA4 and how PDE4 regulates NCOA4 to elucidate how PDE4 regulates autophagy during cerebral ischemia. This will be the focus of our future research. In addition, iron homeostasis in cells is critically controlled by multiple pathways, such as iron uptake, storage, metabolism, and secretion [45]. We focused on the proteins FTH1, FPN, and NCOA4. Whether PDE4 affects other pathways remains to be verified.

GPX4, which is a member of the GPX family, is one the most important negative regulators of ferroptosis [46]. Compared with other GPXs, GPX4 is highly expressed in the brain and especially highly expressed in neurons [32]. GPX4 is able to scavenge intracellular ROS by interrupting lipid peroxidation using GSH as a substrate [32]. In an animal model of transient bilateral common carotid artery ligation, upregulation of GPX4 reduced lipid peroxidation levels in hippocampal tissue and improved cognitive dysfunction [16]. In the present study, we found that the knockdown of GPX4 blocked the enhancing effect of Roflu on cell viability and increased the level of lipid peroxidation in HT-22 cells. These data are consistent with previous studies showing that selenium could counteract hemorrhagic brain injury-induced neuronal ferroptosis by upregulating GPX4 expression [47]. However, the upstream factors regulating the functions of GPX4 within neurons in ischemic brain injury remain to be identified.

In the present study, we found that PDE4 inhibition reduced the cerebral ischemia-induced accumulation of lipid ROS, MDA, and Fe^{2+} in neurons. We then found that GPX4 is essentially involved in the protective effects of PDE4 inhibition against ferroptosis. GPX4 expression is regulated by

several transcription factors, including Nrf-2 and specific protein 1 [33, 47]. Interestingly, our previous study showed that PDE4 inhibition promotes the translocation of Nrf-2 to the nucleus [19]. Therefore, we were interested in whether PDE4 could regulate GPX4 through acting on Nrf-2. We found that the knockdown of Nrf-2 canceled the effects of Roflu on Fe^{2+} levels, GSH levels, and lipid peroxidation. These results suggest that PDE4 inhibition may modulate GPX4 expression through activation of Nrf-2. Interestingly, we also found that Nrf-2 knockdown blocked the Roflu-induced increase in FPN expression. Previous studies indicated that Nrf-2 is a regulator of the iron pool. Transcription of the genes encoding GPX4, FPN, and FTH1 is regulated by the transcription factor Nrf-2 [33]. Upregulation of Nrf-2 enhances resistance to ferroptosis and alleviates brain injury after cerebral ischemia [48]. Hence, it is highly possible that PDE4 inhibition activates Nrf-2 and enhances the level of Nrf-2 in the nucleus, thus promoting the transcription of genes encoding GPX4, FPN, and FTH1 in neuronal cells under cerebral ischemia conditions. We conclude that PDE4 inhibition upregulates GPX4 through activation of Nrf-2, which in turn inhibits neuronal ferroptosis. Nevertheless, the regulation of GPX4, FTH1, and FPN by PDE4 deserves further study in the future, especially in different cell types and at different stages of ischemia. It is important to note that we focused on the effect of PDE4B on ferroptosis in this study. However, the role of other isoforms of PDE4 in ferroptosis has not yet been explored. In particular, PDE4D is considered a risk factor for cerebral ischemia [49], and its role in ferroptosis deserves particular attention in the future. However, we showed that inhibition of PDE4 alleviated cerebral ischemia-induced neuronal ferroptosis through the activation of Nrf-2/GPX4. Still, the mechanism of how PDE4 inhibition affects Nrf-2 and what signaling pathways are involved remain unknown. Our previous studies have indicated that inhibition of PDE4 increases the level of cAMP and activates exchange proteins directly activated by the cAMP (Epac)/protein kinase B (Akt) signaling pathway [9]. Interestingly, Akt is the upstream molecule of Nrf-2, and it has been shown that Akt activity is required for Nrf2-dependent GSH synthesis [50]. Hence, in the present study, we proposed that the effects of PDE4 inhibition on Nrf-2 were probably mediated through the Epac/Akt signaling pathway. More studies are required to further determine how PDE4 acts on Nrf-2 in neuronal cells.

In summary, we revealed that inhibition of PDE4 could significantly inhibit ferroptosis after cerebral ischemia-induced neuronal injury both in vivo and in vitro. PDE4 inhibition primarily exerted protective effects by restoring iron homeostasis and reducing lipid peroxidation by activating the Nrf-2/GPX4 signaling pathway. These findings provide evidence that inhibition of PDE4 is an effective strategy to alleviate neuronal ferroptosis after cerebral ischemia injury, and Roflu is a promising candidate drug for the treatment of cerebral ischemia.

Supplementary Information The online version contains supplementary material available at https://doi.org/10.1007/s12035-024-04495-9.

Author Contributions Conceptualization, H.W. (Haitao Wang); Funding acquisition, H.W. (Haitao Wang) and J.X.; Data Curation, Investigation, and Formal Analysis, K.C., B.X., L.L., H.W. (Huizhen Wen), Q.Z., X.T., and J.W.; Project administration, H.W. (Haitao Wang); Supervision, H.W. (Haitao Wang) and J.X.; Writing – original draft, K.C.; Writing – review & editing, K.C. and H.W. (Hiatao Wang). All authors commented to the manuscript.

Funding This work was supported by the National Natural Science Foundation of China (Nos. 82173802, 82373845, and 82273902), Guangdong Basic and Applied Basic Research Foundation (No. 2022A1515012317).

Data Availability The data that support the findings of this study are available from the corresponding author upon reasonable request.

Declarations

Ethical Approval All experimental procedures were approved by the Laboratory Animal Ethics Committee of Southern Medical University (approval number: SMUL202310009) and performed in compliance with the ethical guidelines of the NIH Guide for the Care and Use of Laboratory Animals (NIH, revised 1996).

Consent to Participate Not applicable.

Competing Interests The authors declare no competing interests.

References

1. Goodman GW, Do TH, Tan C, Ritzel RM (2023) Drivers of chronic pathology following ischemic stroke: a descriptive review. Cell Mol Neurobiol 44(1):7. https://doi.org/10.1007/s10571-023-01437-2
2. Paul S, Candelario-Jalil E (2021) Emerging neuroprotective strategies for the treatment of ischemic stroke: an overview of clinical and preclinical studies. Exp Neurol 335:113518. https://doi.org/10.1016/j.expneurol.2020.113518
3. Liu Q, Shi K, Wang Y, Shi FD (2023) Neurovascular inflammation and complications of thrombolysis therapy in stroke. Stroke 54(10):2688–2697. https://doi.org/10.1161/STROKEAHA.123.044123
4. Delhaye S, Bardoni B (2021) Role of phosphodiesterases in the pathophysiology of neurodevelopmental disorders. Mol Psychiatry 26(9):4570–4582. https://doi.org/10.1038/s41380-020-00997-9
5. Roy D, Balasubramanian S, Krishnamurthy PT, Sola P, Rymbai E (2023) Phosphodiesterase-4 inhibition in Parkinson's disease: molecular insights and therapeutic potential. Cell Mol Neurobiol 43(6):2713–2741. https://doi.org/10.1007/s10571-023-01349-1
6. Li YF, Cheng YF, Huang Y, Conti M, Wilson SP, O'Donnell JM, Zhang HT (2011) Phosphodiesterase-4D knock-out and RNA interference-mediated knock-down enhance memory and increase hippocampal neurogenesis via increased cAMP signaling. J Neurosci 31(1):172–183. https://doi.org/10.1523/JNEUROSCI.5236-10.2011

7. Guo H, Cheng Y, Wang C, Wu J, Zou Z, Niu B, Yu H, Wang H et al (2017) FFPM, a PDE4 inhibitor, reverses learning and memory deficits in APP/PS1 transgenic mice via cAMP/PKA/CREB signaling and anti-inflammatory effects. Neuropharmacology 116:260–269. https://doi.org/10.1016/j.neuropharm.2017.01.004
8. Dong WL, Zhong JH, Chen YQ, Xie JF, Qin YY, Xu JP, Cai NB, Li MF et al (2021) Roflupram protects against rotenone-induced neurotoxicity and facilitates alpha-synuclein degradation in Parkinson's disease models. Acta Pharmacol Sin 42(12):1991–2003. https://doi.org/10.1038/s41401-021-00768-4
9. Xu B, Wang T, Xiao J, Dong W, Wen HZ, Wang X, Qin Y, Cai N et al (2019) FCPR03, a novel phosphodiesterase 4 inhibitor, alleviates cerebral ischemia/reperfusion injury through activation of the AKT/GSK3beta/ beta-catenin signaling pathway. Biochem Pharmacol 163:234–249. https://doi.org/10.1016/j.bcp.2019.02.023
10. Xu B, Xu J, Cai N, Li M, Liu L, Qin Y, Li X, Wang H (2021) Roflumilast prevents ischemic stroke-induced neuronal damage by restricting GSK3beta-mediated oxidative stress and IRE1alpha/TRAF2/JNK pathway. Free Radic Biol Med 163:281–296. https://doi.org/10.1016/j.freeradbiomed.2020.12.018
11. Dixon SJ, Lemberg KM, Lamprecht MR, Skouta R, Zaitsev EM, Gleason CE, Patel DN, Bauer AJ et al (2012) Ferroptosis: an iron-dependent form of nonapoptotic cell death. Cell 149(5):1060–1072. https://doi.org/10.1016/j.cell.2012.03.042
12. Hu X, Bao Y, Li M, Zhang W, Chen C (2024) The role of ferroptosis and its mechanism in ischemic stroke. Exp Neurol 372:114630. https://doi.org/10.1016/j.expneurol.2023.114630
13. Tuo QZ, Lei P, Jackman KA, Li XL, Xiong H, Li XL, Liuyang ZY, Roisman L et al (2017) Tau-mediated iron export prevents ferroptotic damage after ischemic stroke. Mol Psychiatry 22(11):1520–1530. https://doi.org/10.1038/mp.2017.171
14. Zhang L, Bai XY, Sun KY, Li X, Zhang ZQ, Liu YD, Xiang Y, Liu XL (2024) A new perspective in the treatment of ischemic stroke: ferroptosis. Neurochem Res. https://doi.org/10.1007/s11064-023-04096-3
15. Tang D, Chen X, Kang R, Kroemer G (2021) Ferroptosis: molecular mechanisms and health implications. Cell Res 31(2):107–125. https://doi.org/10.1038/s41422-020-00441-1
16. Guan X, Li Z, Zhu S, Cheng M, Ju Y, Ren L, Yang G, Min D (2021) Galangin attenuated cerebral ischemia-reperfusion injury by inhibition of ferroptosis through activating the SLC7A11/GPX4 axis in gerbils. Life Sci 264:118660. https://doi.org/10.1016/j.lfs.2020.118660
17. Li B, Wang W, Li Y, Wang S, Liu H, Xia Z, Gao W, Zhao B (2023) cGAS-STING pathway aggravates early cerebral ischemia-reperfusion injury in mice by activating NCOA4-mediated ferritinophagy. Exp Neurol 359:114269. https://doi.org/10.1016/j.expneurol.2022.114269
18. Wu C, Duan F, Yang R, Dai Y, Chen X, Li S (2023) 15, 16-Dihydrotanshinone I protects against ischemic stroke by inhibiting ferroptosis via the activation of nuclear factor erythroid 2-related factor 2. Phytomedicine 114:154790. https://doi.org/10.1016/j.phymed.2023.154790
19. Xu B, Qin Y, Li D, Cai N, Wu J, Jiang L, Jie L, Zhou Z et al (2020) Inhibition of PDE4 protects neurons against oxygen-glucose deprivation-induced endoplasmic reticulum stress through activation of the Nrf-2/HO-1 pathway. Redox Biol 28:101342. https://doi.org/10.1016/j.redox.2019.101342
20. Zi Y, Wang X, Zi Y, Yu H, Lan Y, Fan Y, Ren C, Liao K et al (2023) Cigarette smoke induces the ROS accumulation and iNOS activation through deactivation of Nrf-2/SIRT3 axis to mediate the human bronchial epithelium ferroptosis. Free Radic Biol Med 200:73–86. https://doi.org/10.1016/j.freeradbiomed.2023.03.002
21. Hatzelmann A, Morcillo EJ, Lungarella G, Adnot S, Sanjar S, Beume R, Schudt C, Tenor H (2010) The preclinical pharmacology of roflumilast–a selective, oral phosphodiesterase 4 inhibitor in development for chronic obstructive pulmonary disease. Pulm Pharmacol Ther 23(4):235–256. https://doi.org/10.1016/j.pupt.2010.03.011
22. Xu BT, Li MF, Chen KC, Li X, Cai NB, Xu JP, Wang HT (2023) Mitofusin-2 mediates cannabidiol-induced neuroprotection against cerebral ischemia in rats. Acta Pharmacol Sin 44(3):499–512. https://doi.org/10.1038/s41401-022-01004-3
23. Cao J, Chen X, Jiang L, Lu B, Yuan M, Zhu D, Zhu H, He Q et al (2020) DJ-1 suppresses ferroptosis through preserving the activity of S-adenosyl homocysteine hydrolase. Nat Commun 11(1):1251. https://doi.org/10.1038/s41467-020-15109-y
24. Zhong J, Li M, Xu J, Dong W, Qin Y, Qiu S, Li X, Wang H (2022) Roflupram attenuates alpha-synuclein-induced cytotoxicity and promotes the mitochondrial translocation of Parkin in SH-SY5Y cells overexpressing A53T mutant alpha-synuclein. Toxicol Appl Pharmacol 436:115859. https://doi.org/10.1016/j.taap.2021.115859
25. Mei H, Zhao L, Li W, Zheng Z, Tang D, Lu X, He Y (2020) Inhibition of ferroptosis protects House Ear Institute-Organ of Corti 1 cells and cochlear hair cells from cisplatin-induced ototoxicity. J Cell Mol Med 24(20):12065–12081. https://doi.org/10.1111/jcmm.15839
26. Fanaei H, Shoorijeh BT, Hafezinouri H, Mirzaei I, Parsi-Moud A (2024) Impact of social isolation on corticosterone release and recovery after stroke in aged rats: a behavioral and biochemical analysis. Exp Gerontol 192:112453. https://doi.org/10.1016/j.exger.2024.112453
27. Tibbo AJ, Baillie GS (2020) Phosphodiesterase 4B: master regulator of brain signaling. Cells 9(5). https://doi.org/10.3390/cells9051254
28. Yan B, Belke D, Gui Y, Chen YX, Jiang ZS, Zheng XL (2023) Pharmacological inhibition of MALT1 (mucosa-associated lymphoid tissue lymphoma translocation protein 1) induces ferroptosis in vascular smooth muscle cells. Cell Death Discov 9(1):456. https://doi.org/10.1038/s41420-023-01748-9
29. Wang T, Yang C, Li Z, Li T, Zhang R, Zhao Y, Cheng T, Zong Z et al (2024) Flavonoid 4,4'-dimethoxychalcone selectively eliminates senescent cells via activating ferritinophagy. Redox Biol 69:103017. https://doi.org/10.1016/j.redox.2023.103017
30. Wang J, Wu N, Peng M, Oyang L, Jiang X, Peng Q, Zhou Y, He Z et al (2023) Ferritinophagy: research advance and clinical significance in cancers. Cell Death Discov 9(1):463. https://doi.org/10.1038/s41420-023-01753-y
31. Li Y, Zeng X, Lu D, Yin M, Shan M, Gao Y (2021) Erastin induces ferroptosis via ferroportin-mediated iron accumulation in endometriosis. Hum Reprod 36(4):951–964. https://doi.org/10.1093/humrep/deaa363
32. Cardoso BR, Hare DJ, Bush AI, Roberts BR (2017) Glutathione peroxidase 4: a new player in neurodegeneration? Mol Psychiatry 22(3):328–335. https://doi.org/10.1038/mp.2016.196
33. Kerins MJ, Ooi A (2018) The roles of NRF2 in modulating cellular iron homeostasis. Antioxid Redox Signal 29(17):1756–1773. https://doi.org/10.1089/ars.2017.7176
34. Granger DN, Kvietys PR (2015) Reperfusion injury and reactive oxygen species: the evolution of a concept. Redox Biol 6:524–551. https://doi.org/10.1016/j.redox.2015.08.020
35. Khan H, Kaur Grewal A, Gurjeet Singh T (2022) Mitochondrial dynamics related neurovascular approaches in cerebral ischemic injury. Mitochondrion 66:54–66. https://doi.org/10.1016/j.mito.2022.08.001
36. Wang Y, Wang M, Liu Y, Tao H, Banerjee S, Srinivasan S, Nemeth E, Czaja MJ et al (2022) Integrated regulation of stress responses, autophagy and survival by altered intracellular iron

stores. Redox Biol 55:102407. https://doi.org/10.1016/j.redox.2022.102407
37. Wang B, Wang Y, Zhang J, Hu C, Jiang J, Li Y, Peng Z (2023) ROS-induced lipid peroxidation modulates cell death outcome: mechanisms behind apoptosis, autophagy, and ferroptosis. Arch Toxicol 97(6):1439–1451. https://doi.org/10.1007/s00204-023-03476-6
38. Zhong J, Dong W, Qin Y, Xie J, Xiao J, Xu J, Wang H (2020) Roflupram exerts neuroprotection via activation of CREB/PGC-1alpha signalling in experimental models of Parkinson's disease. Br J Pharmacol 177(10):2333–2350. https://doi.org/10.1111/bph.14983
39. Yeh SJ, Chen CH, Lin YH, Tsai LK, Lee CW, Tang SC, Jeng JS (2023) Association of ferroptosis with severity and outcomes in acute ischemic stroke patients undergoing endovascular thrombectomy: a case-control study. Mol Neurobiol 60(10):5902–5914. https://doi.org/10.1007/s12035-023-03448-y
40. Xu P, Kong L, Tao C, Zhu Y, Cheng J, Li W, Shen N, Li R et al (2023) Elabela-APJ axis attenuates cerebral ischemia/reperfusion injury by inhibiting neuronal ferroptosis. Free Radic Biol Med 196:171–186. https://doi.org/10.1016/j.freeradbiomed.2023.01.008
41. Wang H, Gaur U, Xiao J, Xu B, Xu J, Zheng W (2018) Targeting phosphodiesterase 4 as a potential therapeutic strategy for enhancing neuroplasticity following ischemic stroke. Int J Biol Sci 14(12):1745–1754. https://doi.org/10.7150/ijbs.26230
42. Munkholm K, Jacoby AS, Vinberg M, Kessing LV (2023) Ferritin as a potential disease marker in patients with bipolar disorder. J Affect Disord 332:247–253. https://doi.org/10.1016/j.jad.2023.04.006
43. Zhao H, Lu Y, Zhang J, Sun Z, Cheng C, Liu Y, Wu L, Zhang M et al (2023) NCOA4 requires a [3Fe-4S] to sense and maintain the iron homeostasis. J Biol Chem 300(2):105612. https://doi.org/10.1016/j.jbc.2023.105612
44. Li C, Sun G, Chen B, Xu L, Ye Y, He J, Bao Z, Zhao P et al (2021) Nuclear receptor coactivator 4-mediated ferritinophagy contributes to cerebral ischemia-induced ferroptosis in ischemic stroke. Pharmacol Res 174:105933. https://doi.org/10.1016/j.phrs.2021.105933
45. Galy B, Conrad M, Muckenthaler M (2023) Mechanisms controlling cellular and systemic iron homeostasis. Nat Rev Mol Cell Biol. https://doi.org/10.1038/s41580-023-00648-1
46. Guo M, Zhu Y, Shi Y, Meng X, Dong X, Zhang H, Wang X, Du M et al (2022) Inhibition of ferroptosis promotes retina ganglion cell survival in experimental optic neuropathies. Redox Biol 58:102541. https://doi.org/10.1016/j.redox.2022.102541
47. Alim I, Caulfield JT, Chen Y, Swarup V, Geschwind DH, Ivanova E, Seravalli J, Ai Y, Sansing LH et al (2019) Selenium drives a transcriptional adaptive program to block ferroptosis and treat stroke. Cell 177(5):1262–1279 e1225. https://doi.org/10.1016/j.cell.2019.03.032
48. Li XN, Shang NY, Kang YY, Sheng N, Lan JQ, Tang JS, Wu L, Zhang JL et al (2024) Caffeic acid alleviates cerebral ischemic injury in rats by resisting ferroptosis via Nrf2 signaling pathway. Acta Pharmacol Sin 45(2):248–267. https://doi.org/10.1038/s41401-023-01177-5
49. Nath M, Swarnkar P, Misra S, Kumar P (2023) Phosphodiesterase 4 D (PDE4D) gene polymorphisms and risk of ischemic stroke: a systematic review and meta-analysis. Acta Neurol Belg 123(6):2085–2110. https://doi.org/10.1007/s13760-023-02218-w
50. Wang L, Chen Y, Sternberg P, Cai J (2008) Essential roles of the PI3 kinase/Akt pathway in regulating Nrf2-dependent antioxidant functions in the RPE. Invest Ophthalmol Vis Sci 49(4):1671–1678. https://doi.org/10.1167/iovs.07-1099